


Concept of power absorbed and lost per electron in surface-wave plasma columns and its contribution to the advanced understanding and modeling of microwave discharges

Michel Moisan ^{*}

Groupe de Physique des Plasmas, Université de Montréal, Montréal H3C 3J7, Québec, Canada

Ivan P. Ganachev

Shibaura Mechatronics Corporation, Yokohama, Japan and Chubu University, Kasugai, Aichi, Japan

Helena Nowakowska 

Institute of Fluid Flow Machinery, Polish Academy of Sciences, Gdansk, Poland



(Received 21 October 2021; accepted 1 August 2022; published 7 October 2022)

Microwave (MW) sustained discharges have distinct advantages over other existing types of discharges in terms of the specific understanding they can provide regarding discharge phenomena and mechanisms. First, only electrons can pick up energy from the discharge E -field since ions cannot respond to rapid oscillations above ≈ 100 MHz. A second remarkable feature of MW discharges is that their plasma sheath is stationary, unlike in radiofrequency (rf) discharges. Furthermore, the sheath voltage is low, so that the electron energy expended to sustain them can be ignored as a first approximation. These characteristics favored the development of the concept of power per electron, which involves determining the respective roles of the power absorbed per electron θ_A and the power lost on a per-electron basis θ_L in the equilibrium relationship between them. This led to establishing the following: (i) In the equilibrium relation of the power per electron ($\theta_A = \theta_L$), the power lost has precedence over the power absorbed, the latter simply adjusting to compensate for the losses. (ii) The value of the power absorbed θ_A , when conforming to compensate for the losses, determines the intensity of the high-frequency E -field in the discharge, the *maintenance field*, construing it as an internal parameter (as opposed to an operator-set). (iii) Ensuring a smaller volume within which power is absorbed (resulting from E -field confinement) compared to the loss volume (plasma) is a way to achieve higher maintenance E -field intensity, thus higher atomic (molecular) excitation and ionization rates, as is the case, for example, with microdischarges. (iv) In pulsed-operated discharges, the E -field intensity is maximum at the very beginning of the pulse and then decreases, eventually reaching stationarity as the pulse time elapses. (v) A significant and more comprehensive similarity law is procured than for direct-current (dc) discharges. (vi) The power per electron concept is valid for all MW discharges. In the case of dc and rf discharges, where ions are also accelerated in the E -field, θ_A is no longer proportional to the E -field intensity: θ_A is then the power necessary to maintain an electron-ion pair in the discharge. It can be used, taking into account the operating conditions (field frequency, gas nature and pressure, and discharge vessel properties), to optimize the power consumed for a given plasma-driven process.

DOI: [10.1103/PhysRevE.106.045202](https://doi.org/10.1103/PhysRevE.106.045202)

I. INTRODUCTION

Microwave¹ (MW) discharges have several advantages over radiofrequency (rf) and direct-current (dc) produced plasmas. Clearly, the presence of electrodes in contact with plasma in dc discharges suffices to rule them out in many applications since their erosion contaminates the discharge. With respect to rf plasmas, the main benefits of using MW plasmas are as follows: (i) As far as applications are concerned, the fact that relatively little energy is spent in ion acceleration

naturally provides higher electron density for a given absorbed power per unit volume, thus favoring faster plasma-driven processes; additionally, it is generally possible to ensure an almost perfect and totally reproducible impedance matching with the MW power generator, which is not the case with rf-induced discharges. (ii) As far as modeling is concerned, it is simpler to describe MW discharges theoretically than dc and rf ones when considering that their power is imparted by the electric field to electrons only: ions do not have time to move around in a microwave field. Furthermore, the Debye length in MW discharges is smaller relative to the plasma volume as well as stationary with respect to the E -field frequency oscillations, while the sheath voltage is low (a few times the average electron energy); therefore, in many cases, the plasma sheath and the electron energy spent to sustain it can be neglected as a satisfactory first approximation.

^{*}michel.moisan@umontreal.ca

¹In the scope of this paper, frequencies above 100 MHz.

Published by the American Physical Society under the terms of the [Creative Commons Attribution 4.0 International](https://creativecommons.org/licenses/by/4.0/) license. Further distribution of this work must maintain attribution to the author(s) and the published article's title, journal citation, and DOI.

The formulation of the concept of *power per electron* began in 1980 with the paper by Glaude *et al.* [1], where proportionality between electron density and absorbed MW power was observed all along a surface-wave (SW) sustained plasma column; the proportionality coefficient was later designated as θ_A , the power absorbed per electron.

Within a few months C.M. Ferreira from the Technical University of Lisbon reproduced the same behavior theoretically. This initiated a series of brilliant theoretical papers elucidating the underlying physics of SW discharges (SWDs). The current paper was started a few years after prof. Ferreira (1948–2014) passed away, with the focus set on the *power per electron* and the *maintenance electric field*, two fundamental concepts central to his work. An energy-balance fluid-plasma-model approach enables us to analyze a wider class of situations, some too complicated to be treated in the plasma-kinetics framework he used.

Once θ_A had been adopted to analyze SWDs, some interesting and often unexpected features followed. For instance, it was unveiled that the intensity of the E -field sustaining a discharge, i.e., the *maintenance field*, is an internal parameter, i.e., it is operator-independent since it intervenes to strictly compensate for the plasma power losses. Moreover, pursuing such a reasoning suggested that confining the E -field enabled raising its intensity in dc, rf, and MW discharges: such a possibility is of the greatest interest in applications since it yields a higher level of atom excitation/ionization and molecule dissociation, allowing us to achieve higher-rate plasma-driven processes [2].

The paper is organized as follows: In Sec. II, surface-wave sustained plasmas (in the MW frequency range) and their features are introduced and thereafter used as the reference MW discharge; Sec. III provides an expression for θ_A , the power absorbed per electron, followed in Sec. IV with the relation of θ_A to the intensity of the MW maintenance electric field E and its use to nonintrusively diagnose the E -field strength, while Sec. V discusses contributions to the power lost per electron (designated θ_{Lc}), essentially through electron-neutral collisions. Section VI presents, within the specific context of the power-per-electron concept, an expression for the (stationary) power balance, focusing on the difference between discharges with homogeneous and localized electron heating, the latter characterized by a power-deposition volume smaller than the plasma volume. Section VII extends the use of the θ parameter to SWD similarity laws, while Sec. VIII contains a summary and conclusion. The Appendix is devoted to a comparison with the power balance in capacitively coupled rf discharges, where, in contrast to SWDs, the high-frequency E -field accelerates both electrons and ions.

II. SURFACE-WAVE SUSTAINED PLASMA COLUMNS

The definition of the power absorbed per electron θ_A and its corresponding properties stemmed both from observations and modeling advances achieved specifically on SW sustained plasma columns, so first the necessary background information on SWDs is presented. Discharges supported by the electromagnetic (EM) field of a propagating surface wave are the reference plasma in the current study.

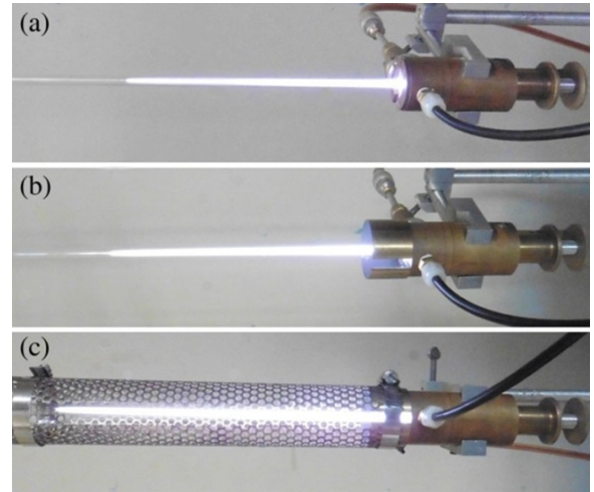


FIG. 1. Photographs showing the different plasma columns obtained in a 6/8 (mm) inner/outer diameter (i.d./o.d.) fused silica tube with a surfatron (MW field-applicator) operating at 915 MHz: (a) in free air; (b) with the discharge tube coaxially enclosed in a conducting cylinder [Faraday cage (FC)] of 22.5 mm radius preventing electromagnetic (EM) leakage from affecting the laboratory measurements [2]; the length of the cage is 30 mm, the minimum length to prevent any undue EM emission; (c) with again a Faraday cage of 22.5 mm radius but 305 mm length, longer than the plasma column. The power coupled to the surfatron from the MW generator is 300 W in each photo. The axial slit of the FC allows field intensity measurement and optical emission spectroscopy along the plasma column without any EM field escaping into the room [5].

A. Achieving long plasma columns inside a dielectric tube utilizing localized MW field applicators

Surfatron. Figure 1 shows photos of a plasma column generated from a surfatron MW field-applicator located at one end of the discharge tube [3,4]. The discharges depicted were obtained in argon gas under atmospheric pressure operated at a frequency $f = 915$ MHz in an open-ended dielectric tube, the latter either standing alone in free-space (a) or partially (b) and fully (c) coaxially surrounded by a conducting cylindrical enclosure, a Faraday cage (FC), to reduce or prevent, respectively, MW radiation in the room [5].

Surfaguide. Figure 2 schematically describes the setup required to produce a plasma column with a surfaguide [3,6], a MW field applicator of relatively small axial extension along the discharge tube. In this example, the plasma column is generated at 2450 MHz in argon gas at atmospheric pressure inside a 2/6 mm inner/outer diameter (i.d./o.d.) fused silica tube surrounded by a 54 mm inner radius FC. The plasma column extends almost symmetrically from the surfaguide launching interstice provided the gas flow rate is moderate, i.e., 250–500 standard cubic centimeters per minute (sccm) [7], whereas the surfatron plasma column in Fig. 1 emerges on one side of the launcher.

MW power operation of a surfatron at 2450 MHz must be limited to about 300 W to avoid damage to the coaxial feeder cable, whereas a surfaguide, where MW power is carried by a waveguide, can easily handle 6 kW [6]. For better impedance matching to the MW generator, the narrow wall of

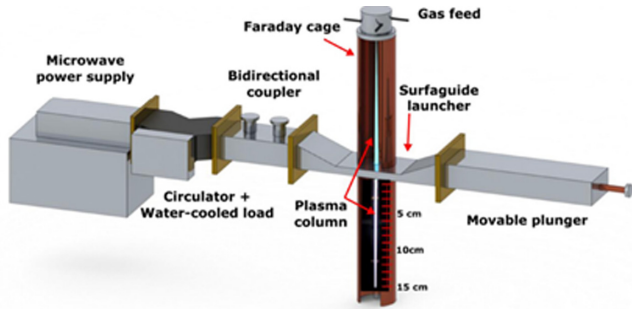


FIG. 2. Schematic description of the auxiliary equipment utilized to sustain a plasma column with a surfatron field-applicator. Working conditions in the present case are 2450 MHz at 300 W in argon gas in a discharge tube with i.d./o.d. 2/10 mm, at atmospheric pressure at a flow rate of 250–500 sccm [7]. The inner radius of the FC, 54 mm, is above a circular waveguide cutoff.

the rectangular waveguide is tapered so that the impedance of the surfatron is close to the characteristic impedance of the surface wave plasma column regarded as a transmission line [2]. A family of similar field applicators with different attributes (field frequency, impedance matching means) is discussed in [3].

B. Axial distribution of electron density along the plasma column generated with the surfatron: Identification of the portion sustained by a SW

The plasma columns exhibited in Fig. 1 consist (although it is not visibly apparent) of two successive axial segments: the first one, starting at the surfatron gap (EM-field leaking interstice), results from ionization by the EM radiation developed by the field-applicator acting as an antenna [5], while the next section, farther along the plasma column, is sustained by the propagation of an EM surface wave, guided along the discharge-tube/plasma-column interface, and thus inducing a

surface-wave discharge. The axial variation of electron density along these two successive plasma column segments is illustrated, although represented differently, in Figs. 3(a) and 3(b) in the absence of any FC.

Figure 3(a) shows the axial distribution of the radially averaged electron density along the plasma column plotted as a function of the position from the surfatron slit, while in Fig. 3(b) it is plotted as a function of the position from the end of the plasma column, revealing in this case a different and more informative picture: it shows that the increase in applied MW power, while extending the length of the plasma column, does not modify the previously existing axial electron density gradient. In both figures, a distinct part of the axial distribution of the plasma column electron density varies linearly, a key feature related to the propagation of a surface wave sustaining a SWD [2,8].²

The EM field applicator acts as an antenna. It is responsible for producing plasma in the initial part of the column. This segment is characterized by its curved shape (upward or downward), as can be seen in Figs. 3(a) and 3(b), before the SWD develops. Its axial extent does not change as the MW power coupled to the surfatron varies, and this is actually a fraction of the wavelength in vacuum, λ_0 . At 2450 MHz, this fraction is ≈ 0.23 for a surfatron and ≈ 0.06 for a surfatron [5]. The EM radiation emanating from the field-applicator penetrates the (MW transparent) dielectric discharge tube, ionizing the gas within it.

The antenna-type EM radiation excites a nonguided wave (space wave), which spreads outwardly. It generates the EM field emission detected in the laboratory, affecting measurements and potentially harmful to the op-

²The fact that in Fig. 3(a) the electron density axial distribution for 270 W curves down toward the end of the plasma column instead of remaining linear is an experimental flaw, confirmed by later measurements [8].

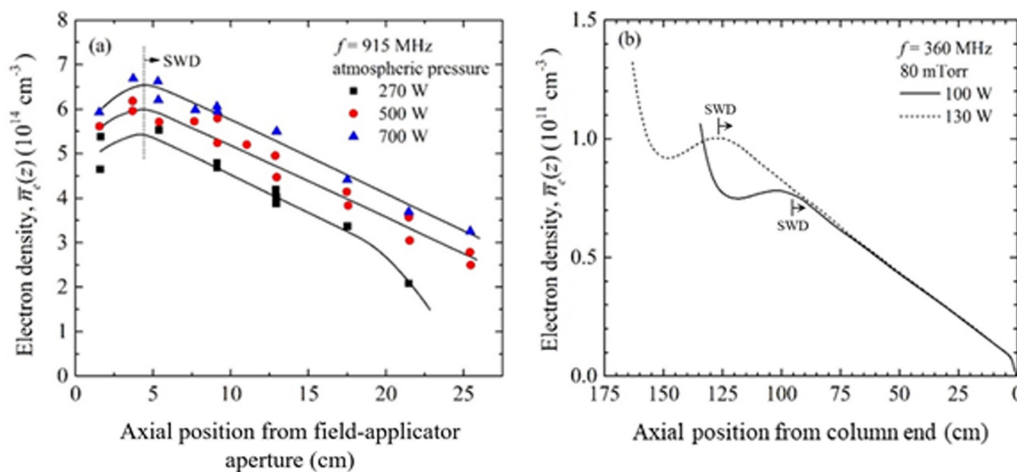


FIG. 3. Measured radially averaged electron density \bar{n}_e along an argon plasma column sustained by the electric field of EM waves, initially launched from a surfatron field-applicator, as a function of axial distance plotted in (a) from the field applicator radiating interstice for a discharge tube of 1.94 mm inner diameter at atmospheric pressure and at a field frequency of 915 MHz [9], and in (b) from the end of a 25-mm-diam plasma column, at reduced pressure (≈ 10 Pa) and sustained at 360 MHz. The leftmost data point in Fig. 3(a) is located at approximately 1–2 mm from the surfatron gap. In both figures, the arrow (with the SWD label) points at the beginning of the specific SWD section, which follows the antenna-type EM radiation sector of the field-applicator.

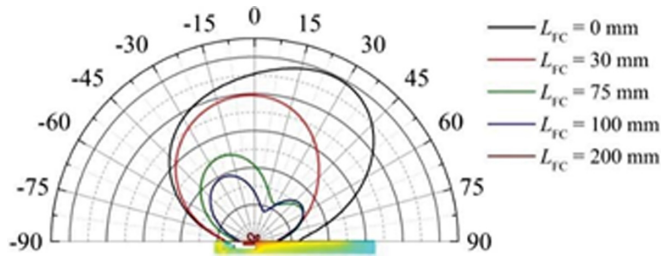


FIG. 4. Calculated power radiation pattern generated by the 915 MHz surfatron field-applicator for different L_{FC} lengths of the Faraday cage operating at the waveguide cutoff (Fig. 1). The plasma column is oriented along the polar axis ($\Theta = -90^\circ$ to 90°), where Θ is the elevation angle. The intensity of the main lobe decreases with increasing L_{FC} and tilts backwards as space-wave losses are reduced (absorbed power of 300 W is assumed) [5].

erator's health (above a certain level of mW/cm^2). Such spurious EM field radiation can be avoided by coaxially surrounding the plasma column with a conducting cylinder, a Faraday cage (FC). Operating with a sufficiently small FC radius [Eq. (1) below] prevents waveguide-mode propagation in the FC considered as a circular waveguide.

Faraday cage waveguide cutoff condition. When the radius R of a circular waveguide is equal to or smaller than

$$R_{(\text{co})}[\text{mm}] = 8.790 \times 10^4 / f[\text{MHz}], \quad (1)$$

no wave can propagate within it. This happens because the fundamental TE_{11} mode is then under a waveguide cutoff condition [10]. At 915 and 2450 MHz, this corresponds to $R_{(\text{co})} = 96.1$ and 35.9 mm, respectively. A surface wave can nevertheless propagate and maintain the plasma even if it is surrounded by a FC in cutoff condition: the surface wave is guided along the discharge tube and its plasma column, which serve as propagation medium.

Figure 4 shows the calculated radiation pattern generated by the 915 MHz surfatron field-applicator for different L_{FC} lengths of the Faraday cage operating at the waveguide cutoff [Figs. 1(b) and 1(c)]. The main radiation lobe is directed forwards at an angle of about 30° to the column axis for $L_{FC} = 0$, but it tilts backward as L_{FC} increases (details are in [11]). Most importantly, the radiated power decreases with increasing L_{FC} . Increasing L_{FC} results in a longer plasma column, as can be seen in Figs. 1(b) and 1(c) compared to Fig. 1(a) [5]. Under similar operating conditions, approximately 30% more electrons are being produced in Fig. 1(c) than in Fig. 1(a), yielding a longer plasma column [5].

The surface-wave supported plasma column itself is particularly convenient as an antenna for communications, in contrast to the space-wave region at the EM launcher exit. In fact, nonmetal SW monopole antennas can be configured and operated for defense communications in such a way that their existence lasts less than a few microseconds, as a valuable alternative to metal retractable antennas [11–14].

C. Linear distribution of electron density along SWDs and its dependence on operating conditions

The first SWD fully identified as such in the literature can be found in a 1970 paper by Tuma [15]. A family of efficient SW launchers intended to sustain such plasma columns was worked out over the 1973–1990 period at the Université de Montréal together with reports on the properties, mostly experimental, of surface-wave discharges; see, e.g., Ref. [1]. The initial known attempt at modeling plasma columns sustained by a slowly propagating EM surface wave was due to Aliev, Boev, and Shivarova [16], who examined a plasma in the thin cylinder approximation laid in vacuum. They considered the propagating SW wave to be weakly damped and of the TM type. The electron density was assumed to be proportional to the wave power absorbed along the plasma column and high enough that power flowing within the plasma column could be neglected, the wave power concentrated almost entirely in the vacuum surrounding the plasma. Conservation of the flowing energy yielded the axial gradient of electron density along the plasma column as

$$\frac{d\bar{n}_e}{dz} = C_1 \frac{\omega v_m}{R}, \quad (2)$$

where C_1 is a constant, $\omega = 2\pi f$ is the (angular) wave frequency, v_m is the average electron-neutral collision frequency for momentum transfer, and R is the inner radius of the discharge tube. This predicted linear profile of plasma density is actually observed all along the SW plasma column, including up to its very end [1,8]. The dependence (2) of the axial gradient of electron density on $v_m \omega / R$ is confirmed both by experiments and numerical calculations [8,17]. This indeed differs from the prediction of many models, e.g., [18,19], which produce axial distributions of electron density that do not end linearly (but rather with a bump). This is due, however, to the models overestimating the coupling between discharge kinetics and Maxwell equations, especially near the column end, where many of the premises of the respective models do not hold.³ Still, density measurements processed through least-squares regression indicate linearity until the last measurable points. In a recent work still in progress [8], it is established through review of experimental data that the density gradient is entirely and solely set by the *operating conditions*, namely f , the nature and pressure of the gas (strictly speaking, the number density N) through v_m , and R , in accordance with Eq. (2). This will be exemplified with experimental results below.

Figure 5 shows the measured axial distribution of electron density referred to the end of the SWD column: (a) for a variety of gas pressures (related to v_m) at a given field frequency, and (b) for a variety of EM field frequencies at a given gas pressure (given v_m). In Fig. 5(a), the various curved line segments of electron density occurring at axial positions before the SWD linear line belong to the antenna-type radiation region of the applicator, as already discussed in Fig. 3.

³The column ends when the SW can no longer propagate, be it because electron density is under its cutoff [Eq. (3) below], or because high gas pressure prevents it.

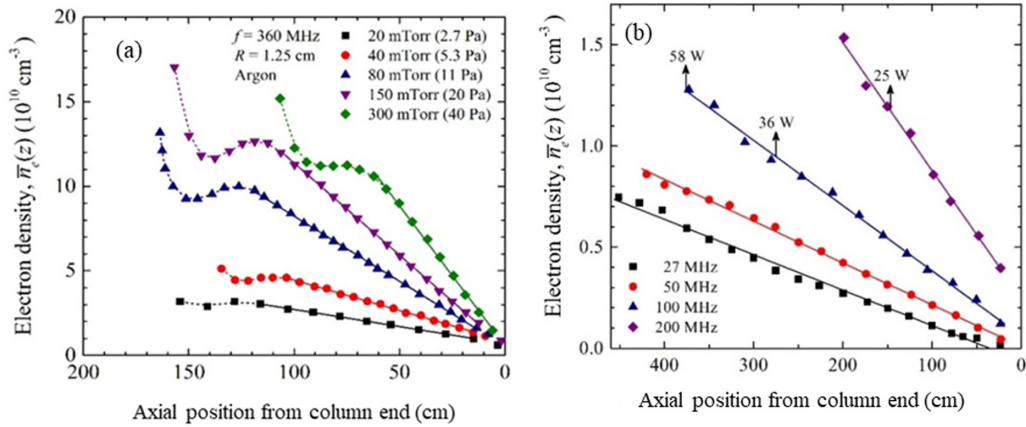


FIG. 5. Measured axial variation of the radially averaged electron density $\bar{n}_e(z)$ referred to the end of the plasma column in a SWD sustained with a surfatron field-applicator in argon: (a) at 360 MHz at five different gas pressures in a tube of 25 mm i.d. [1], showing the curved plasma segment produced by the surfatron radiation-field followed by the SWD plasma column, recognizable by the linear decay of $\bar{n}_e(z)$ ⁴; (b) at four different field frequencies at a pressure of 30 mTorr (≈ 4 Pa) such that $v_m/\omega < 1$ in a tube of 64 mm i.d. [20], with the $\bar{n}_e(z)$ values restricted to the SWD portion of the plasma column.

The length of the radiation section (curved part) behaves as follows: (i) It increases with gas pressure, saturating at about 80 mTorr; (ii) it does not increase with power [Fig. 3(a)], except for eventually very low power not sufficient to get to the linear SWD zone (not shown); (iii) it decreases with increasing frequency [compare Fig. 3(a) with 3(b)]; (iv) it is shorter with a surfaguide field-applicator than with a surfatron [5]. Figure 5(b) has been limited to the linear SWD part of the plasma column. Note again that the column length increases with power while preserving the axial gradient of the electron density, as illustrated at 100 MHz when the power is varied from 36 to 58 W [2].

Figure 6 illustrates finally the variation of the axial gradient of the electron density following three increasing values of R .

In summary, Figs. 5(a), 5(b), and 6 confirm the increase in the fixed axial gradient of electron density $d\bar{n}_e/dz$ with the increase of f , v_m (through p), and $1/R$, in good agreement with (2).

The minimum electron density of a SW plasma column is reached at its end and it increases as the field frequency and gas pressure are raised. An important feature of SWDs is the occurrence of a minimum electron density, manifested at the end of their plasma column. It truly defines the end of the plasma column because, below this value, the SW no longer propagates along it. This minimum value increases with SW frequency. In the low-pressure case ($v_m/\omega \ll 1$), SW propagation stops whenever the electron density becomes lower than the resonance density $\bar{n}_{e(re)}$, which is given by [21]

$$\bar{n}_{e(re)} [\text{cm}^{-3}] \approx 1.2 \times 10^4 (1 + \epsilon_d) (f[\text{MHz}])^2, \quad (3)$$

where ϵ_d is the relative permittivity of the dielectric at the plasma boundary (often denoted ϵ_g in the case this dielectric is glass). The electron density thus rises as the square of the applied field frequency f . Furthermore, when the gas pressure is high enough such that v_m/ω is no longer much less than unity, then due to a lack of power to sustain the discharge, the SW plasma column terminates at an electron density always greater than $\bar{n}_{e(re)}$. In all cases, there is an increase in the minimum SWD electron density with f^2 and eventually p , as illustrated in Figs. 5(b) and 5(a), respectively.

Gas pressure p and the underlying gas density and temperature. In all the figures reported in this work (except Fig. 19), the quantity p refers to the experimental, measured, pressure of the gas. Since the number density N of the gas depends

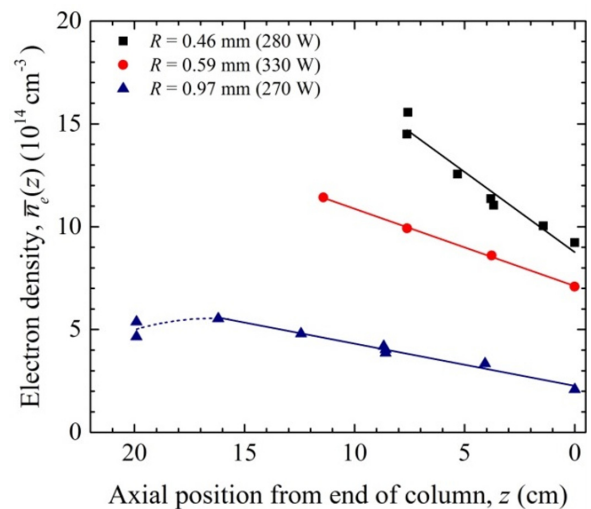


FIG. 6. Measured axial distribution of the radially averaged electron density, displayed from the end of the plasma column sustained by a SW at 915 MHz in (fused silica) discharge tubes of three different inner radii R , in argon gas at atmospheric pressure (after [9]).

⁴Excellent linearity of the whole axial distribution of electron density along SWDs is supported by high coefficients of determination r^2 in least-squares regressions [8], as, for example, in Fig. 5(b), where for successively increasing frequency, $r^2 = 0.990, 0.999, 0.998$, and 0.998 .

on its temperature T as $N = p/k_B T$ (k_B is the Boltzmann constant), p does not reflect the full physics of the discharge: in fact, it is possible to reach the same pressure value with different couples N and T . All collision frequencies, although often considered proportional to p , are strictly speaking not proportional to it, but to N , and therefore N is the appropriate variable for modeling and also when expressing a similarity law. To establish the value of N from p , T must be known. A shortcut to this is to imply some standard temperature T_0 (for example, 300 K) and use *converted* gas pressure $p' = Nk_B T_0$ as representative of N .

As a rule, in SWDs the gas temperature T depends on the discharge tube inner radius, the gas pressure, the flow rate, and on the operating field frequency. T remains approximately constant from the field applicator along the plasma column before decreasing toward the column end. Its decay at the column end is limited because the corresponding axial distribution of electron density (electron collisions are responsible for gas heating) cannot fall below a minimum n_e value set by (3). As a result, for given operating conditions, T along SWDs can be assumed constant as a working approximation. Possible values of T are as follows: (i) at low gas pressures ($v_m/\omega \ll 1$), for example, at 300 mTorr in argon at $f = 360$ MHz [Fig. 5(a)] accounting for a maximum available power of 65 W, the plasma column requires only 6 W per 10 cm, leading to T not much above room temperature (300 K); (ii) at pressures in the 0.5–5 Torr range in He, for example, $T \approx 900$ –1800 K [22]; (iii) at atmospheric pressure, in a discharge tube with a small enough inner diameter (≤ 1.5 mm) to avoid plasma radial contraction in argon, T is in the 1400–1600 K range according to [23] and 1250–1500 K as reported by [24]. Having on hand p from measurements, N from calculations, and some estimate for T , one can easily switch to converted pressure p' as done in Fig. 19.

III. POWER ABSORBED PER ELECTRON, θ_A

Initially, in Glaude *et al.* [1], the letter θ simply referred to the observed proportionality constant between the total number of electrons on any given axial section of a MW SW-supported plasma column and the power absorbed on that same given plasma segment. Later, Chaker *et al.* [25] demonstrated that the inverse of the proportionality constant of Glaude *et al.* [1] was in fact “the average power required to create an electron.” This observation became even more important after Chaker *et al.* [25] found that, under ambipolar diffusion conditions, the value of θ along a SWD was “independent of the input power.” In the articles that followed, it became customary to keep θ (its capital letter Θ for some) to designate the power absorbed in a plasma column sustained by a surface wave.

A. Defining θ_A along the SWD empirically from power measurements

It was observed in Fig. 5(b) that adding an amount of power ΔP to a preexisting SWD of power P provides an additional plasma column length Δz . This increases the total number $n_{\text{tot}} = \int_0^z \bar{n}_e(z') S(z') dz'$ of electrons by $\Delta(n_{\text{tot}}) \approx$

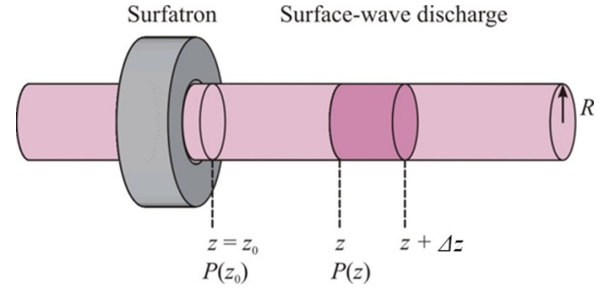


FIG. 7. Schematic description showing that the power $\Delta P(z)$ extracted from the wave power flow $P(z)$ along the $z, z + \Delta z$ segment is absorbed in the discharge gas within that same axial segment. $P(z_0)$ is the initial power flow value at the beginning of the SWD past the initial space-wave radiation zone [2].

$\bar{n}_e(z) S(z) \Delta z$, where $S(z)$ is the tube inner cross-sectional area, and the overbar indicates averaging over S . Therefore, a sequence of power increase ΔP accompanied by measurement of the electron density profiles $\bar{n}_e(z)$ allows us to define, from experiment, the power absorbed per electron, $\bar{\theta}_A(z)$ as the proportionality constant between the increments of power ΔP and the additional number of electrons $\Delta(n_{\text{tot}}) = \int_z^{z+\Delta z} \bar{n}_e(z') S(z') dz' \approx \bar{n}_e(z) S(z) \Delta z$:

$$\theta_A = \Delta P / \Delta(n_{\text{tot}}) \approx \Delta P / [\bar{n}_e(z) S(z) \Delta z]. \quad (4)$$

Switching from finite to infinitesimal small increments, (4) can then be written as

$$dP_A(z) / dz = \theta_A(z) \bar{n}_e(z) S(z), \quad (5)$$

where dP_A refers to the power absorbed in the discharge. This empirical relation ignores the wave properties.

The experimental value of θ_A . It can be ascertained from its definition (4) by determining the amount of power spent (absorbed) within the cylindrical plasma section bounded by z and $z + \Delta z$ (say $\Delta z = 10$ –20 mm depending on the axial resolution looked for) and of cross-sectional area S , as illustrated in Fig. 7. The quantity thus procured over the corresponding plasma volume yields the (cross-section averaged) power density. Dividing this number by the (measured) average electron density in the considered Δz segment yields θ_A , which value can then be assigned to axial position $z + \Delta z/2$. Figure 10 is an illustration of θ_A values obtained in this way along a SW plasma column.

B. Relation of θ_A to the SW attenuation

Expression (5) has been obtained from MW power absorption along a given segment of the SW plasma columns without referring to the attenuation of the wave power. It can be linked to the transfer of power from the propagating wave to the plasma column by considering Fig. 7, which exhibits a graphical representation of the power flow along a SWD. It shows that the plasma column generated within the $z, z + \Delta z$ segment results from the power flow diverted and absorbed from the wave along this same axial segment. $P(z)$ is the wave power flow available in the plane perpendicular to the tube axis at z : it thus includes the power flow contribution extending radially from $r = R$ (inner radius of the discharge

tube) up to $r = \infty$, where r is the radial position away from the tube axis.

The power flow available at z , $P(z)$, results from the wave power loss from z_0 up to axial position z . Its value can be expressed in terms of the wave-power attenuation coefficient $2\alpha(z)$, which generally depends on $\bar{n}_e(z)$ [denoted as $\alpha[\bar{n}_e(z)]$],⁵ yielding

$$P(z) = P(z_0) \exp \left\{ -2 \int_{z_0}^z \alpha[\bar{n}_e(z)] dz \right\}. \quad (6)$$

From here, one can write down $-dP(z)$, the amount of power subtracted from the wave-power flow over the $z, z + dz$ segment, as

$$-dP(z) = 2\alpha[\bar{n}_e(z)]P(z)dz. \quad (7)$$

This should be equal to the total power absorbed in the same segment, which, taken from (5), yields

$$2\alpha[\bar{n}_e(z)]P(z)dz = \theta_A[\bar{n}_e(z)] \bar{n}_e(z)S(z)dz. \quad (8)$$

This provides the relation between $\bar{\theta}_A(z)$ and the wave attenuation:

$$\bar{\theta}_A(z) = 2\alpha[\bar{n}_e(z)] P(z)/[\bar{n}_e(z) S(z)]. \quad (9)$$

Expressions (2), (5), (7), and (9) show that SWDs offer some distinguishing advantages for modeling and collecting experimental data in a consistent way. More specifically: (i) Be it in the rf or MW domain, the SW power flowing over any given axial section of the discharge tube is spent within the corresponding segment of plasma column. As a result, (ii) the number of electrons generated over a given differential axial segment (volume) of the plasma column is proportional to the rf or MW power absorbed within it. It allows us to achieve a highly locally resolved power balance and analysis of all the discharge features. (iii) For SWDs generated in the MW frequency domain, the energy acquired by electrons in the \mathbf{E} -field drives ionization of the discharge gas simply through electron collisions with heavy particles. (iv) Since the axial gradient of the electron density of SWDs depends only on operating conditions (2), data gathered under the same operating conditions in different laboratories are bound to be identical [8], eliminating the need for agreeing on a “standard setup” with which to be compared.

C. Local transfer of SW power to plasma (skin effect) and electron energy spreading

An EM wave does not fully penetrate plasma when its frequency f is lower than $f_{pe} = \omega_{pe}/2\pi$, the electron plasma frequency, as is the case with SWs. In fact, electrons distribute their charge and current to shield out the electromagnetic wave, resulting in the skin effect phenomenon [26]. Only a small (twice the electron to atom mass ratio m_e/M) part of the energy acquired by electrons in the MW \mathbf{E} -field is lost in a single elastic collision. In fact, in the specific case of low-temperature and partially ionized plasmas (as in SWDs), electrons can travel over a large (energy relaxation) length

before they lose a substantial part of their energy. As a result, when the discharge dimension is small compared with the energy relaxation length, although the wave power is locally absorbed, the EEDF has to be described by a nonlocal model: it depends on the entire profile of the electric field and not on its local value [27,28]. It should be further noticed that in many SWDs the tube radius R is smaller than the skin depth ($\sim c/\omega_{pe}$, where c is the speed of light in vacuum). In this case, the \mathbf{E} -field is practically radially homogeneous, and one can forget about the skin effect. In modeling, this is referred to as the “thin cylinder approximation” ($\omega_{pe}R/c \ll 1$).

IV. THE MAINTENANCE ELECTRIC FIELD AND θ_A

In a discharge sustained by a MW field in steady state, the value of θ_A (eventually properly averaged) is determined only by operating discharge conditions, such as the gas pressure and field frequency. It turns out that in MW SWDs, there is a simple intrinsic relation between the power absorbed per electron θ_A and the \mathbf{E} -field intensity, as demonstrated in this section. This means that the \mathbf{E} -field intensity, contrary to common sense intuition, cannot be increased at will by turning up the power. This field is called the *maintenance field* to distinguish it from the *breakdown field*, where the situation is far from steady state.

Starting with the power P_A taken from the \mathbf{E} -field by the electrons, per unit volume, in the case of plasmas with an assumed uniform electron density n_e , one can write

$$P_A \equiv n_e \theta_A = \mathbf{J} \cdot \mathbf{E}, \quad (10)$$

where \mathbf{J} is the electron-current density, which constitutes a generalization of Ohm’s law (for the above expression and the rest of this section, details can be found in Sec. 2.2 of [26]).

dc discharge case. The power θ_A is related to the work done by electrons in the discharge electric field. It can be shown to be given by

$$\theta_A(E) = \frac{e^2}{m_e \nu_m} E^2, \quad (11)$$

where ν_m is the average (macroscopic) electron-neutral collision frequency for momentum transfer, averaged over the electron energy distribution function (EEDF).

HF discharges (zero applied magnetic field). In the case of high-frequency (HF designates both rf and MW) \mathbf{E} -fields, the matter of energy transfer must be posed differently from that in dc discharges since the electric field is periodic. The electron is accelerated in one direction under the influence of the electric field for the first half of the periodic cycle, then in the opposite direction for its second half:⁶ on average over a cycle, the work achieved by an electron in an HF field is zero. Only collisions, interrupting the periodic motion, allow the electron a net energy gain from the HF electric field.

⁵The axial value of electron density $\bar{n}_e(z)$ depends solely on its distance to the column end, not on $P(z)$; see Fig. 3(b).

⁶The amplitude of oscillation (or excursion) of an electron in the HF electric field is assumed to be smaller than the discharge vessel’s shortest dimensions (for example, the radius R in a long cylindrical plasma column). This is generally the case for EM fields with frequencies above 1 MHz.

The motion of charged particles in an EM \mathbf{E} -field creates a conduction current. For an electron density n_e , the current density can be written as

$$\mathbf{J} = -n_e e \mathbf{v}, \quad (12)$$

where \mathbf{v} , the EEDF averaged (vector) electron velocity, in complex form to account for collisional momentum losses, is [26]

$$\mathbf{v} = \frac{-e \mathbf{E}}{m_e (\nu_m + i\omega)}. \quad (13)$$

In a linear conducting medium,

$$\mathbf{J} = \sigma \mathbf{E}, \quad (14)$$

where σ is the electrical conductivity (scalar in the absence of static magnetic field), and from (12)–(14):

$$\sigma = \frac{n_e e^2}{m_e (\nu_m + i\omega)}. \quad (15)$$

From (10), after time averaging, $\theta_A \equiv P_A/n_e = \frac{1}{2} \text{Re}(\mathbf{E} \cdot \mathbf{J}^*)/n_e$ is found to be

$$\theta_A = (1/2) \text{Re}(-e \mathbf{E} \cdot \mathbf{v}^*) = \frac{e^2 \overline{E^2}}{m_e} \frac{\nu_m}{\nu_m^2 + \omega^2}, \quad (16)$$

where Re provides the real part of complex quantities, the asterisk indicates complex conjugation, and $\overline{E^2} \equiv E_0^2/2$ is the mean-squared value of the electric field amplitude. When MW power is applied initially, E_0 is the *breakdown* field, whereas under steady-state conditions, the value of E_0 (maintenance field) is basically set by losses; see Sec. VI A.

In contrast to planar dc discharges, the \mathbf{E} -field intensity in SW sustained plasmas is not radially constant, but decreases from the tube walls to the axis: this phenomenon is akin to the attenuation of an EM wave entering a conductive material (skin effect). Under these conditions, integrating the value of θ_A across a transverse section of the plasma column leads to a radially averaged value of θ_A that should strictly be designated as $\bar{\theta}_A$, nonetheless hereafter denoted θ_A for simplicity. Still, with the widely used narrow tubes, the thin cylinder approximation ($\omega_{pe} R/c \ll 1$) is justified, and the \mathbf{E} -field can be treated as radially uniform,

Effective electric field. In their analysis of so-called HF discharges, Allis and Brown [29] introduced E_e^2 , the effective electric field intensity:

$$E_e^2 \equiv \overline{E^2} \frac{\nu^2}{\nu^2 + \omega^2}, \quad (17)$$

where ν is the electron-neutral collision frequency for momentum transfer, generally speaking dependent on electron energy ε . E_e can be used to reduce the number of variables in the Boltzmann kinetic equation for the electrons and is especially convenient when considering discharges in hydrogen and helium,⁷ because for them the dependence of ν on ε is negligible, and ν can be treated as a constant.

Ferreira and Loureiro [30] considered E_e^2 as “a useful parameter for the modeling of HF gaseous discharge characteristics”⁸ in macroscopic similarity laws, replacing ν in (17) by its EEDF averaged value ν_m to deal with argon gas, where ν varies considerably with electron energy ε :

$$E_e^2 = \overline{E^2} \frac{\nu_m^2}{\nu_m^2 + \omega^2}. \quad (18)$$

Noteworthy then is the fact that the expression E_e^2/ν_m has a structure similar to that of θ_A in (16), notwithstanding the physical constants e^2/m_e . This explains the “usefulness” (and recognized success) of using the notion of effective electric field intensity in modeling HF discharges. The fact that θ_A [hence the \mathbf{E} -field intensity through (16)] is observed to be constant along a MW SW plasma column, except at its very end, is the underlying reason for the success of the effective \mathbf{E} -field intensity approach.

HF discharges in an external magnetic field. To estimate θ_A in magnetized plasmas, and in particular at and close to electron cyclotron resonance (ECR), assume a plasma sustained by a planar EM wave with its \mathbf{E} -field oriented parallel to the y axis [so that its only nonzero component is $E_y = E_0 \exp(i\omega t)$] and subjected to a static and uniform magnetic field \mathbf{B} directed along z (a uniform axial magnetic field is the configuration most widely used with SWDs). Since in magnetized plasmas the \mathbf{B} -field acts on the electron velocity in a plane perpendicular to \mathbf{B} , the resulting electrical conductivity is not the scalar value (15), but a tensor $\bar{\sigma}$ of rank 2 with five nonzero components. The tensor matrix is [26]

$$\begin{aligned} \bar{\sigma} &= \begin{pmatrix} \sigma_{xx} & \sigma_{xy} & 0 \\ \sigma_{yx} & \sigma_{yy} & 0 \\ 0 & 0 & \sigma_{zz} \end{pmatrix} \\ &= -\frac{i n_e e^2}{m_e \omega} \begin{pmatrix} \frac{\omega^2}{\omega^2 - \omega_{ce}^2} & \frac{i\omega \omega_{ce}}{\omega^2 - \omega_{ce}^2} & 0 \\ -\frac{i\omega \omega_{ce}}{\omega^2 - \omega_{ce}^2} & \frac{\omega^2}{\omega^2 - \omega_{ce}^2} & 0 \\ 0 & 0 & 1 \end{pmatrix} \end{aligned} \quad (19)$$

for collisionless and

$$\bar{\sigma} = \frac{n_e e^2}{m_e (i\omega + \nu_m)} \begin{pmatrix} \frac{(i\omega + \nu_m)^2}{(i\omega + \nu_m)^2 + \omega_{ce}^2} & -\frac{(i\omega + \nu_m) \omega_{ce}}{(i\omega + \nu_m)^2 + \omega_{ce}^2} & 0 \\ \frac{(i\omega + \nu_m) \omega_{ce}}{(i\omega + \nu_m)^2 + \omega_{ce}^2} & \frac{(i\omega + \nu_m)^2}{(i\omega + \nu_m)^2 + \omega_{ce}^2} & 0 \\ 0 & 0 & 1 \end{pmatrix} \quad (20)$$

for collisional plasma, where (20) is obtained from (19) by the substitution $i\omega \rightarrow (i\omega + \nu_m)$. The electron current $\mathbf{J} \equiv -n_e e \mathbf{v}$ has then two nonzero components:

$$J_x \equiv -n_e e v_x = \sigma_{xy} E_y \quad \text{and} \quad J_y \equiv -n_e e v_y = \sigma_{yy} E_y, \quad (21)$$

of which only J_y (the component directed along \mathbf{E}) contributes to the scalar product $\mathbf{J} \cdot \mathbf{E}^*$ determining the absorbed power density:

$$P_A = (1/2) \text{Re}(\mathbf{J} \cdot \mathbf{E}^*) = (1/2) \text{Re}(J_y E_y^*) = (1/2) E_0^2 \text{Re}(\sigma_{yy}). \quad (22)$$

⁷Although He is a noble gas, it does not give rise to the Ramsauer effect.

⁸Expression (17) is also a way of reducing the number of independent parameters when modeling [30].

From here then, after working out the real part of σ_{yy} ,

$$\text{Re}(\sigma_{yy}) = \frac{e^2 n_e v_m}{m_e} \frac{1}{2} \left[\frac{1}{(\omega - \omega_{ce})^2 + v_m^2} + \frac{1}{(\omega + \omega_{ce})^2 + v_m^2} \right], \quad (23)$$

we obtain [26]

$$\theta_A \equiv \frac{P_A}{n_e} = -\frac{e}{2} \text{Re}(v_y E_y^*) = \frac{e^2 E_0^2}{2 v_m m_e} \left[\frac{1}{2} \frac{v_m^2}{(\omega - \omega_{ce})^2 + v_m^2} + \frac{1}{2} \frac{v_m^2}{(\omega + \omega_{ce})^2 + v_m^2} \right]. \quad (24)$$

Note that (24) transforms into (16) when $\omega_{ce} = 0$.

V. THE POWER LOST ON A PER ELECTRON BASIS, θ_L

The power subtracted from the wave electric field is acquired by electrons only, provided the field frequency exceeds 100 MHz (ions then do not respond to it). In cold plasmas, this power is lost mainly through various types of collision of the electrons with heavy particles, a possible form of which per electron is [31]

$$\theta_{Lc}(\langle \varepsilon \rangle) = \frac{2m_e}{M} \langle v_{el}(\varepsilon) \varepsilon \rangle + \sum_j \langle v_j(\varepsilon) \varepsilon_j \rangle + \langle v_i(\varepsilon) \varepsilon_i \rangle, \quad (25)$$

where the symbol $v_{el}(\varepsilon)$ denotes the electron-energy-dependent elastic collision frequency for electrons of energy ε with energy transfer $(2m_e/M)\varepsilon$ to the heavy particles of mass M , and v_j and v_i are the electron-energy-dependent collision frequencies generating atomic (molecular) excitation to level j (threshold energy ε_j) or ionization (threshold energy ε_i), respectively; the brackets $\langle \rangle$ indicate averaging over the EEDF. Relationship (25) illustrates the case of excitation and ionization from the ground state (*direct collisions*) only. In the case of Maxwellian EEDF, the average values in (25) are entirely determined by the sole electron temperature T_e and the gas pressure. In general, $\theta_{Lc}(\langle \varepsilon \rangle)$ is an increasing function of $\langle \varepsilon \rangle$ [26]. In situations in which the gas pressure is high enough that the assumption of only “direct collisions from ground level” fails due to too frequent collisions, multistep excitation and ionization processes allow low-energy electrons to contribute significantly to energy transfer, so that these additional possibilities must be taken into account too (see also Sec. VII C).

Ultimately, the power thus passed on from electrons to heavy particles is mainly lost in light emission (photons) through deexcitation or radiative electron-ion recombination and in discharge gas heating, finally transferred out through the tube wall.

The phenomena described in (25) acting on the value of θ_{Lc} can be complemented to account further for the following:

(i) The dependence of the EEDF upon the level of electron density (appraised by the degree of ionization, and influencing the EEDF mostly via the amount of electron-electron collisions) and on the way the charged particles created in the volume disappear from the discharge: in addition to diffusion towards the walls of the vessel on which ions and electrons readily recombine to form neutral atoms, there is

also electron-ion recombination in the volume of the plasma [discussed later on with Eq. (33)].

(ii) When multistep excitation processes are becoming important, metastable atomic states, for example, have to be added to direct excitation [32]. Multistep ionization generally reduces the average electron energy, hence θ_A (see also Fig. 20).

(iii) Some amount of the power gained by electrons in the wave electric field is ultimately lost as they hit the walls ($\sim 2k_B T_e$ per electron-ion pair created), in sustaining sheaths, and in establishing the ambipolar dc field (denoted as P_d in [33]). As already mentioned, the sheath voltage in MW discharges is low [$\sim (1/2)(k_B T_e/e) \ln(M/m_e)$], so that the electron energy spent (per electron) to sustain the sheath is small (a few times the average electron energy) and can be neglected in a first approximation. As for the energy lost to sustain the ambipolar field (“presheath”), it is equal to the energy gained by ions accelerated in the presheath to Bohm velocity $(k_B T_e/M)^{1/2}$, i.e., to kinetic energy $k_B T_e/2$. This amounts to an energy loss of $k_B T_e/2$ per electron, even less than the energy lost in supporting the sheath. Both of these contributions are small compared to θ_{Lc} (except eventually at very low pressures and high electron temperatures, usually not encountered in SWDs) and are therefore neglected in the current concept paper for brevity. Still, they could be kept without changing anything significantly because, similarly to the collisional losses (25), in SWDs they too depend only on electron temperature T_e (strictly speaking EEDF). Nonetheless, one can keep in mind that the total electron power per electron θ_L encompasses θ_{Lc} , and is slightly larger than it.

VI. POWER BALANCE IN THE POWER-PER-ELECTRON SPECIFIC CONTEXT

A. The case of homogeneous E -field electron heating

The balance between the power extracted from the MW electromagnetic field (fully supplied to electrons only), and the power that electrons lose (in collisions with the gas atoms/molecules, at the walls, as well as in building up sheaths and the dc ambipolar electric field), governs its steady state. In the case of narrow-tube SW sustained plasma columns, a perfect example of a discharge with homogeneous electron heating, the power conservation principle on a per electron basis and under steady-state conditions reads

$$\theta_A = \theta_L. \quad (26)$$

Indeed, if the power θ_A were less than θ_L , the discharge would extinguish. If, on the contrary, θ_A was greater than θ_L , the electron density would increase, contradicting the assumption of a stationary state [34,35]. Therefore, in steady state and the case of homogeneous electron heating, one need not distinguish between θ_A and θ_L and can denote their common value as θ .

Enlightening insight into discharge mechanisms, often ignored or overlooked, can be revealed from the *per-electron-power balance* (26) when acknowledging that the quantity θ_L has precedence over θ_A in this relationship, as pointed out in [2]. Two demonstrations are given below in this subsection. As a result, the absorbed power per electron θ_A strictly adjusts, under steady-state conditions, to compensate for the power losses θ_L [2]. Taking advantage of this reasoning, calling on

(16) for θ_A , from (26) there comes (for SWDs with zero dc magnetic field)

$$\theta_A \equiv \frac{e^2}{m_e} \frac{v_m}{v_m^2 + \omega^2} \overline{E^2} = \theta_L, \quad (27)$$

which implies that, under steady-state conditions, the \mathbf{E} -field intensity is set by losses, in other words that it is an *internal parameter*, i.e., self-consistently adjusted, not operator-set [2]. By the same token, the field intensity can also be designated as the *maintenance field*.

In magnetized SWDs with uniform magnetic field, the expression for θ_A on the left of Eq. (27) has to be replaced with the absorbed power per electron in magnetic field (24), again stating that the maintenance field is an internal parameter, set by the losses and the discharge conditions (in this case with the addition of the electron cyclotron ratio ω_{ce}/ω).

The fact that the \mathbf{E} -field is an internal (and not externally set) parameter will be exemplified in two interesting and counterintuitive effects.

Demonstration 1: Comparison of absorbed power per electron at electron cyclotron resonance (ECR) (collisionless) and very close to it (collisional).

The fact that θ_L has a prominent role over θ_A , i.e., that θ_A has to compensate for θ_L , can be demonstrated by examining the gradual shift from collisional to collisionless (ECR) electron heating in a magnetized SW plasma column. The power taken from the \mathbf{E} -field per electron is then found to remain on the same θ_A/p versus pR line despite the transition to a qualitatively different type of power intake: in other words, the value of θ_A does not depend on the way power is supplied to maintain plasma.

To show this, let us consider a SW plasma column sustained in an axially directed static and uniform magnetic field \mathbf{B} : an additional parameter of discharge operation is then the electron cyclotron angular frequency $\omega_{ce} = eB/m_e$. When B is tuned so that $\omega_{ce} = \omega$ (first ECR condition) but the gas pressure is not low enough to satisfy the second ECR condition ($v_m/\omega \ll 1$), the absorption of MW power by electron collisions with heavy particles (collisional absorption) is still significant. However, when the gas pressure is further reduced to values such that the second ECR condition $v_m/\omega \ll 1$ is also met, ECR (collisionless) absorption takes over.

Figure 8 displays θ_A/p measurements made as functions of the product pR in an axially magnetized surface-wave sustained plasma column. Consider the case in which gas pressure p is continuously decreased such that power transfer progressively shifts from collisional to collisionless electron heating. The θ_A/p versus pR data points in Fig. 8 are observed to stay on the same $\omega_{ce}/\omega = 1$ straight line as the product pR is lowered, resulting in collisionless power absorption consecutively supplanting collisional power intake: no significant deviation (within the uncertainty margin) of the data points from the $\omega_{ce}/\omega = 1$ straight line is noticed in the figure as the situation evolves continuously toward fulfilling simultaneously both ECR conditions ($\omega_{ce}/\omega = 1$, $v_m/\omega \ll 1$). It can thus be concluded that the way energy is delivered to electrons has no influence on the power balance (26). In other words, the way of compensating for the power lost θ_L (collisional or collisionless electron heating) is immaterial to its value.

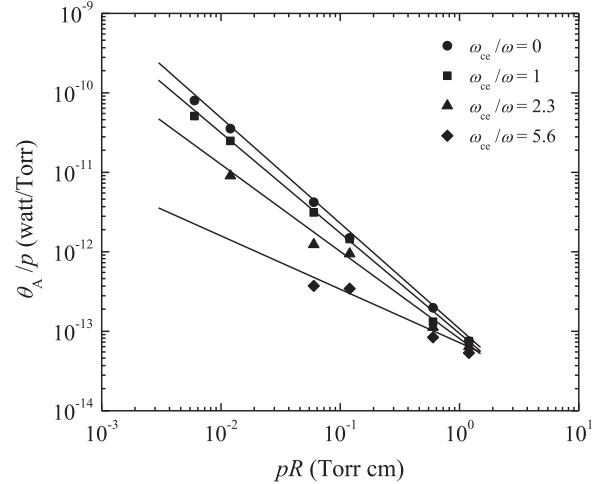


FIG. 8. Measured absorbed MW power per electron as a function of the product pR in a surface-wave sustained argon discharge, operated at the field frequency $\omega/2\pi = 600$ MHz, and immersed in a static magnetic field \mathbf{B} directed along the plasma column axis, considering different values of the ratio ω_{ce}/ω (including first ECR condition $\omega_{ce}/\omega = 1$). The discharge tube inner radius is $R = 13$ mm while p is varied between 5×10^{-3} and 1 Torr (≈ 0.67 –133 Pa) in order to achieve the pR values plotted in the figure [36]. The EM surface wave propagates along this magnetized plasma column on the HE_{01} fundamental mode [37].

A further (classical) point to be observed in Fig. 8 is that the power absorbed per electron θ_A , at a given pR value, decreases monotonically with stronger \mathbf{B} -field, as expressed through the increase in ω_{ce} . The major effect of the magnetic field is in reducing the transverse ambipolar diffusion and therefore making possible sustaining the SWD at lower ionization rates, i.e., lower electron temperatures. The lower electron temperature then results in lower values of θ_L , as per Eq. (25), and hence of θ_A , as per Eq. (26).

Demonstration 2: Minimum \mathbf{E} -field intensity at ECR in SWDs

This is another specific (and unanticipated) outcome of the precedence of θ_L over θ_A . There has long been a general belief that the intensity of the EM \mathbf{E} -field passes through a maximum at ECR, a conviction supported by the fact that atomic/molecular excitation/ionization was recorded to be the greatest when, under appropriate ECR gas pressure conditions, the ω_{ce}/ω ratio is tuned to unity. Some authors, such as Allis [38], claimed, based on the mentioned observations, that the value of the \mathbf{E} -field intensity in the plasma should thus be “amplified” under ECR conditions. No field intensity measurement, however, was ever provided to endorse this point.

To show that this interpretation is incorrect in a *uniform* magnetic field, recall the relation (24) between θ_A and E_0^2 for the case when a dc magnetic field is imposed on the plasma. This expression for θ_A , with presumed (for the moment) constant intensity $E_0^2/2 = \overline{E^2}$, clearly goes through a maximum at $\omega_{ce} = \omega$. However, as shown experimentally in Fig. 8, θ_A does not experience any extremum when encompassing ECR conditions. To get to the origin of the contradiction, let us recall that, according to (22), the power absorbed per electron

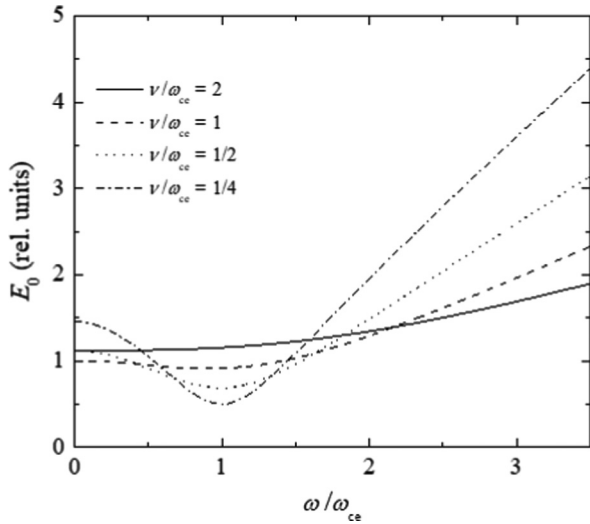


FIG. 9. Calculated value of E_0 as a function of the ω/ω_{ce} ratio, assuming a planar EM wave propagating along a uniform and axially magnetized plasma column, and accounting for the fact that θ_A as defined by Eq. (28), is constant. Four values of ν/ω_{ce} are considered, indicating that E_0^2 , the intensity of the wave \mathbf{E} -field at ECR frequency, goes through a minimum, more pronounced as the ν/ω_{ce} ratio gets smaller [2].

is

$$\theta_A \equiv \frac{P_A}{n_e} = \frac{E_0^2}{2n_e} \operatorname{Re}(\sigma_{yy}). \quad (28)$$

The expression for $\operatorname{Re}(\sigma_{yy})$ in the vicinity of resonance, retaining only the ECR frequency-condition term ($\omega_{ce} \approx \omega$) in (23), is

$$\operatorname{Re}(\sigma_{yy}) = \frac{n_e e^2}{m_e} \left[\frac{1}{2} \frac{v_m}{(\omega - \omega_{ce})^2 + \nu_m^2} \right]. \quad (29)$$

The electron-conductivity tensor component (29) evidently passes through a maximum at the ECR frequency condition, while, as demonstrated experimentally (Fig. 8), the value of θ_A only decreases monotonously with increasing pR . As a result, the quantity E_0^2 in (28) must go through a minimum to compensate for the maximum of $\operatorname{Re}(\sigma_{yy})$ at ECR. Figure 9 shows the results of such calculations, the minimum of E_0 deepening as ν_m/ω_{ce} is lowered. This issue was reported for the first time in [39], specifically with regard to the analysis of the power-per-electron concept in magnetized high-frequency plasmas, with further calculations later on in [2].

As to the higher excitation/ionization rates often observed in magnetized plasmas of different kinds at ECR, they are mostly due to nonuniformity of \mathbf{B} reducing the volume where ECR occurs to a fraction of the entire plasma volume (a situation not encountered with SWDs, where a uniform magnetic field is usual). With nonuniform \mathbf{B} , one gets another example of an inhomogeneous discharge with confined (localized) \mathbf{E} -field electron heating, resulting in high ionization and

excitation rates in this small localized volume, as explained in the next subsection.⁹

B. The case of localized electron heating (high-intensity \mathbf{E} -field conditions)

As already argued, the value of the \mathbf{E} -field intensity is set by the power losses θ_A through their balance (27) with absorbed power θ_L . However, the balance of absorbed and lost power need not be met at each point in the plasma; it suffices that the *volume integrals* of absorbed and lost power be equal. Since $\theta_L (\approx \theta_{Lc})$ is determined (25) by the electron energy, over which we have no direct control, the only remaining way to act on the \mathbf{E} -field strength stands on the power absorption side, leading to the idea to reduce the volume in which microwave power is “deposited” in the discharge. As developed in what follows, decreasing the portion of plasma volume in which MW power is absorbed prompts raising the intensity of the maintenance \mathbf{E} -field. It should be clear that this cannot be achieved with a SWD because, essentially, the power absorbed (from the wave) over any given segment of the plasma column is always spent within that same plasma segment (Sec. III B), a situation referred to in Sec. VI A as discharge with homogeneous electron heating.

It is well known that the increase of the rf or MW power transferred to a discharge does not raise the intensity of its sustaining field but rather leads to a higher electron density. As a solution to this, it has been considered to improve the quality factor of the resonant cavity through which a discharge tube goes, thus subjecting it to a higher \mathbf{E} -field intensity as the Q factor is greater.¹⁰ This was forgetting that the field strength at steady state adjusts itself to strictly compensate for the power losses, which remain the same (per electron) regardless of the way in which the \mathbf{E} -field is established. On the other hand, practical results in raising the \mathbf{E} -field intensity have already been reported (e.g., microdischarges [41]) but without giving a guiding principle that allows for this realization. The basic principle of the method was apparently presented and documented for the first time only recently in [40]. Being able to increase the intensity of the maintenance \mathbf{E} -field is of the utmost interest for both fundamental research and plasma-driven applications, as it allows, for example, a higher rate of atomic/molecular excitation and ionization and molecular dissociation than with homogeneous \mathbf{E} -field electron heating, ultimately leading to higher efficiency of plasma-driven processes.

⁹In this way of thinking, the nonuniformity of the magnetic field in Helicon rf discharges and the limited extent of their antennas (small power deposition volume) can be held responsible for the higher local plasma densities obtained compared with other rf sources of similar powers [39].

¹⁰Many still believe that sustaining a microwave discharge with a resonant cavity having a high Q factor will provide higher field amplitude in the discharge than with other types of microwave field applicators. In fact, ignition of the discharge should be easier (Sec. VIC) but, under steady-state conditions, the maintenance \mathbf{E} -field intensity, for given operating conditions, remains the same as with any other means of discharge since the \mathbf{E} -field intensity is set by plasma losses [40].

1. Power balance in discharges with localized electron heating

Increasing the intensity of the maintenance E -field requires, as argued, reducing the volume V_i in which EM power is absorbed (designated as the inner volume, in fact the power deposition volume) relative to the total volume V_t that the plasma occupies.

Such a nonlocal power balance can be analyzed in an insightful way with the θ_A and θ_L parameters, assumed for simplicity to be spatially uniform over V_i and V_t , respectively. The global power balance, neglecting losses to the sheath and the ambipolar dc field ($\theta_L \approx \theta_{Lc}$), requires that

$$\theta_A \bar{n}_{ei} V_i = \theta_L \bar{n}_{et} V_t, \quad (30)$$

where \bar{n}_{ei} and \bar{n}_{et} are the average electron densities in the power absorption (inner) and diffusion (total plasma) volumes, respectively. Since $\bar{n}_{ei} V_i$ (the number of electrons in the inner volume) is smaller than $\bar{n}_{et} V_t$ (the number of electrons in the entire plasma),¹¹ it imposes that

$$\theta_A / \theta_{Lc} > 1. \quad (31)$$

A larger θ_A value means, according to (16),¹² a higher intensity of the maintenance E -field than under homogeneous electron heating.

Discharges with localized electron heating can be realized in different ways, requiring at any rate that the E -field be confined within a smaller volume than that of the plasma, as is the case with the field applicator described later in Sec. VI B 3.

2. Probing the E -field intensity along SWD using θ_A :

The column end problem

A specific advantage of the power-per-electron concept in the case of MW discharges is that it allows us, as mentioned, to determine experimentally, with precision, the value of the E -field intensity through measurements of θ_A and the use of relation (16) [42]. On the other hand, attempts to directly evaluate the E -field intensity with an antenna are intrusive and, therefore, inaccurate. Figure 10 reports the measured values of θ_A along a SWD plasma column in the ambipolar diffusion regime. It shows that (i) the power cost to maintain an electron in the discharge is the same all along the plasma column, except at its very end; (ii) the sudden increase of θ_A at the SW plasma column end reveals a corresponding jump in the E -field intensity [2].

The sudden increase in E -field intensity observed at the end of the SW plasma column can be explained by appealing to the considerations above regarding discharges with localized electron heating. Indeed, the volume of the very last axial differential segment of the column in which power is absorbed (inner volume) is smaller than the (total) volume formed by the plasma diffusing axially outward (region without E -field), resulting in a higher local value of θ_A and, hence, of the E -field intensity (Sec. VI B 1).

¹¹Only the “confined electrons” (inner volume) are subjected to E -field heating.

¹²Recall: valid for MW discharges only.

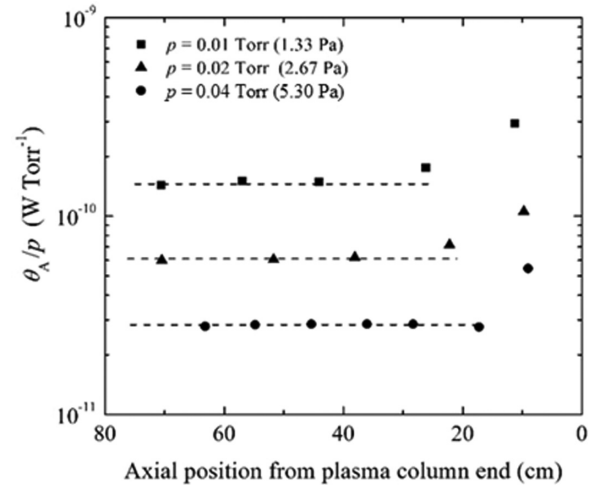


FIG. 10. Experimental values of θ_A/p as functions of axial position from the end of the SW plasma column sustained at 200 MHz for three different gas pressures p . For a given gas pressure, θ_A is observed not to vary with axial position except at the very end of the column where it makes a jump [42].

3. Localized electron heating in an inhomogeneous MW discharge designed for strong E -field

Figure 11(a) presents a schematic drawing of a microwave E -field applicator yielding from the outset an inhomogeneous discharge in terms of E -field configuration [43]. Two circular (copper) plates acting as radiating disk antennas serve to supply the discharge with microwave power. These antennas are each placed across the tube diameter defining the discharge axis [z -axis in Figs. 11(b) and 11(c)], which is perpendicular to the tube axis in Fig. 11(a). Each antenna is provided with MW power through a straight segment of a 50 Ω semirigid coaxial cable (≈ 2.2 mm outside diameter), the bare inner conductor of which extends beyond the outer conductor by a few mm with its tip soldered to the back center of the antenna’s circular surface. Both antennas lean against the outer wall of the discharge tube, which is made from fused silica, a dielectric material well transparent to microwave field. The power supplied by the MW generator is split into two equal portions (with a 3 dB power divider) and, at the same time, a 180° phase difference between these two antennas is set up with a phase shifter ($\Delta\phi$). The latter is tuned for a minimum intensity of the MW power signal detected at its frequency f_0 on a spectrum analyzer with an electric-field antenna (straight wire) positioned at 90° from the z -axis [Fig. 11(a)]. Such a setting ensures that the resulting E -field pattern emerging from the antennas is mainly directed along the z -axis, and therefore mostly confined within a virtual cylinder, defined by the common axis of the two disk antennas and extending all along the discharge tube diameter. The antennas are held in place by a cylindrical metallic (brass) structure, closed at both ends to avoid radiation in the room. This assembly also constitutes a resonant cavity used to determine the electron density in the discharge by the frequency shift of its TM_{010} mode [44].

Figures 11(b) and 11(c) present the simplified axisymmetric 2D configuration elected for modeling, along with artist’s views of the discharge luminosity: the cylindrical absorption

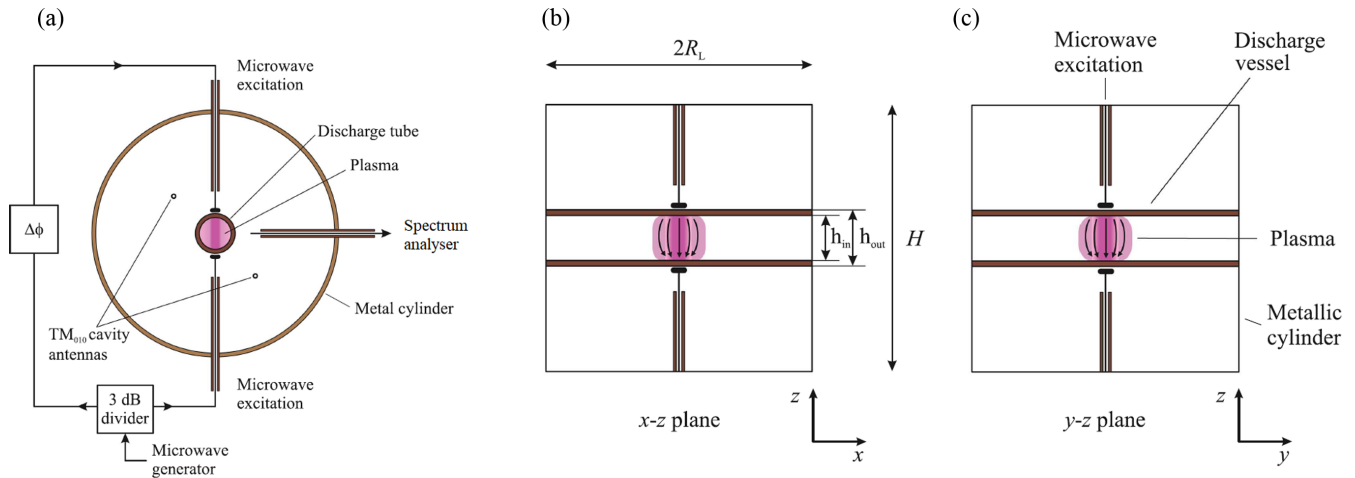


FIG. 11. (a) Schematic cross-sectional view of the microwave field-applicator utilized for achieving a high intensity maintenance E -field in the discharge. Two circular copper plates radiate MW power sustaining the discharge (see the text and [43] for details); (b) and (c) are views of the simplified axisymmetric 2D configuration of the field-applicator chosen for calculating the discharge properties, displaying the MW power absorption zone (violet) and the diffusion volume contour (pink), full lines showing accordingly the direction of the E -field in the two perpendicular cut planes [2]; z is the axis of symmetry.

(inner) volume (violet denotes higher plasma density) and the external contour of the diffusion plasma (total) volume (pink for lower plasma density); the solid lines in Figs. 11(b) and 11(c) indicate the direction of the E -field. The numerical calculations presented below have been performed with argon gas pressure of 0.1 Torr (13.3 Pa) and a 2.45 GHz applied field frequency f_0 with less than 5 W of total MW power.

E -field as a function of absorbed MW power. Numerical simulation of the properties of the MW discharge arrangement described above was conducted using COMSOL MULTIPHYSICS™ software with rf (implying here microwaves) and plasma modules (details are in [40] and [2]). There exist two electron density regions over which the E -field reaches high-intensity values. These zones are termed underdense and overdense with respect to the critical electron density (the density at which $f_{pe} = f_0$, where f_{pe} is the electron plasma frequency), according to whether f_{pe} is smaller or larger than f_0 , respectively. The kind of electron-plasma oscillations occurring in each of these zones was figured out by considering the possibility of wave propagation within or along the virtual cylinder confining the E -field. In the underdense case, the electron wave is a “volume” (unguided) wave excited inside the plasma cylinder, where $f_{pe} < f_0$. On the other hand, in the overdense case, the electron wave is an EM surface wave (guided wave) propagating along the plasma cylinder for $f_0 \approx f_{pe}(1 + \epsilon_r)^{-1/2}$, where ϵ_r is the relative permittivity of the dielectric medium [in the present situation, a comparatively low-density plasma, hence $\epsilon_r \approx 1$ and $(1 + \epsilon_r)^{1/2} \approx \sqrt{2}$] which surrounds the high-electron-density plasma cylinder [40]. Figure 12, besides delineating the underdense and overdense regions as functions of absorbed MW power, confirms that the more confined the E -field (antenna plates of smaller and smaller radius with respect to plasma radius), the higher the E -field intensity in both electron density regions, with the highest intensity occurring in the overdense zone.

Number of electrons as a function of absorbed MW power. The absolute number of electrons in the whole plasma volume, for given discharge operating conditions and additionally MW power, is found in the calculations to be independent of the degree of confinement of the E -field sustaining the discharge. This is because the operating conditions of the discharge fully determine the plasma properties, including total power losses [8], while power absorption (limited to the inner volume) has no choice but to compensate strictly and passively for this power losses, as already underlined (Sec. VI A). Therefore, since the properties of the plasma are

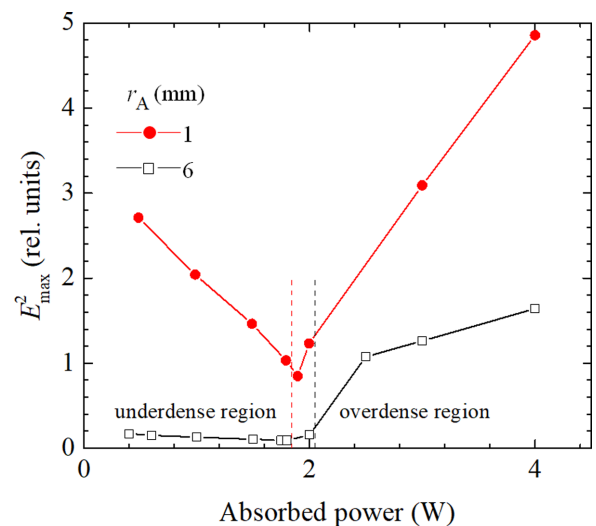


FIG. 12. Calculated maximum value of the E -field intensity within the whole analyzed volume as a function of increasing absorbed MW power (hence increasing electron density) at 2.45 GHz and 0.1 Torr (13.3 Pa) in argon gas, for two radii r_A of the antenna radiating plates [other conditions: $R_L = 10$ mm, $h_{in} = 8$ mm, as in Fig. 11(b)] [2].

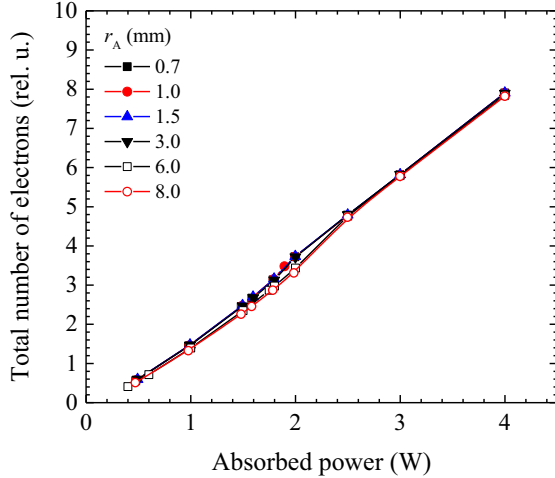


FIG. 13. Calculated total number of electrons in the discharge arrangement of Figs. 11(b) and 11(c) as a function of MW absorbed power for various antenna-plate radii, the degree of E -field confinement increasing as the plate radius r_A decreases. Same operating conditions as in Fig. 12 [2].

not affected as the E -field confinement is varied, it was to be expected that the total number of electrons in the discharge would remain constant. The calculations, reported in Fig. 13, confirm that this is the case: the total number of electrons in the plasma does not vary regardless of the antenna-plate radius to plasma radius ratio. Although the E -field intensity increases as the inner volume is reduced (Fig. 12), the discharge does not become more power-efficient: the power lost per electron, being set by plasma losses, remains the same. This is another facet of the demonstration, achieved under ECR conditions (Sec. VI A), that the nature of the power intake has no influence on plasma losses, an original outcome of the current model.

4. Parametric resonance excitation of ion plasma frequency oscillations as an indication of a high-intensity E -field in a discharge under localized electron heating

In this subsection, we discuss the EM emission spectrum measured in the experiment from Fig. 11(a), as shown in Fig. 14, and we present the arguments underlying its interpretation as proof of a high-intensity E -field, as should be expected for such localized electron heating.

First, let us start by recalling that free electron plasma oscillations (*electron plasmons* with frequency f_{pe}) can be easily excited and detected by disturbing the plasma in a suitable way (e.g., by a beam of electrons emitted from a hot filament [45]), but that this is not the case for ion plasma oscillations (*ion plasmons* with frequency f_{pi}): the excitation of ion plasmons requires special conditions. The qualitatively different behavior for electron and ion plasmons is caused by the huge mass difference between ions and electrons. Indeed, it is easy to have electron oscillations at a background of almost static ions due to the large inertia of the latter. In contrast, there is no way to achieve a background of almost static electrons for the ion oscillations: the superlight electrons move immediately (at the electron thermal velocity v_e) in

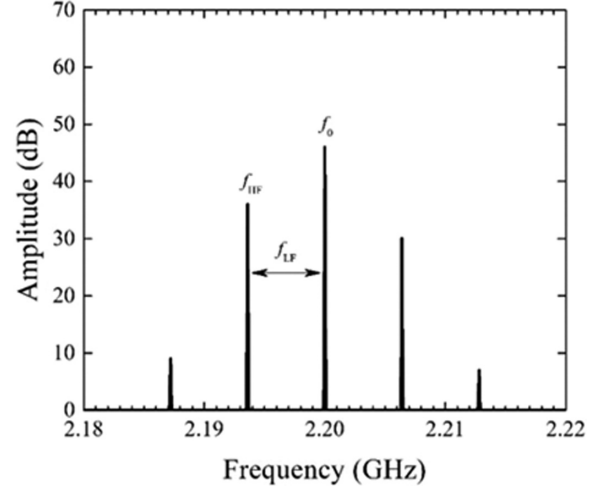


FIG. 14. Typical microwave spectrum recorded from the discharge arrangement [Fig. 11(a)] in the overdense electron density region when periodic oscillations are parametrically excited. Pump frequency f_0 is 2.20 GHz and the first left side-band f_{HF} yields $f_{LF} = f_0 - f_{HF}$ according to the frequency selection rule (32). Krypton gas pressure is 10 mTorr (≈ 1.3 Pa) in a 9.6 mm i.d. tube (details in [2] and [50]). The base-line has been drawn just above noise level.

response to any ion displacement to restore the Boltzmann equilibrium of electrostatic field and electron density. This electron realignment prevents the emergence of any long-scale low-frequency electrostatic field needed for the ion oscillations. This could be overcome if the ions were to move at speeds higher than the electron thermal velocity v_e , but this is hardly possible due to the large ion inertia.

Still, there is one feasible option for enabling ion plasma oscillations: decouple the electron and ion movements by means of a strong external electric field forcing the electrons to oscillate independently of the ion movements. To achieve this, the external field (of frequency $f_0 = \omega_0/2\pi$ and amplitude E_0) must cause the electrons to oscillate with directed electron oscillation amplitude (“*electron excursion*”) $x = eE_0/(m_e\omega_0^2)$ much longer than the Debye length λ_{De} [46]. The electrons are forced to move with large swings and are not left to realign in response to the ion displacement. As a result, the electrostatic field of the ion oscillations is left unshielded, enabling their buildup. Therefore, the detection of a phenomenon related to the excitation of ion plasma oscillations can be used as an indication of a strong high-frequency electric field.

Both electron and ion plasma oscillations need a stimulus to be launched and observed. In the simpler case of the electron plasma oscillations, excitation is possible by forcibly disturbing the plasma, using, e.g., a beam of hot electrons. In such a case, the frequency range of oscillations indicates the electron density range in the disturbed plasma volume (and it can be used for electron density measurement [45]). The frequency spectrum is somehow broad, because the disturbance cannot be strictly localized to one point, so that f_{pe} picks up the plasma inhomogeneity of the disturbed region. A narrow (single-line) spectrum corresponding to electron plasma oscillations coming out from an otherwise

inhomogeneous plasma is possible only through resonance: applying a high-frequency external electric field of frequency f_0 . With such excitation, electron plasma oscillations are activated only in regions where the local electron plasma frequency is equal to the frequency of the externally applied field, and the oscillation spectrum has a single line at $f_{pe} = f_0$.

This thinking can be extended to the excitation of ion plasma oscillations, provided the electron excursion x is longer than the Debye length. In such conditions, ion plasma oscillations become possible, too, and the plasma has now two natural (eigen)frequencies f_{pe} and f_{pi} . Again, a narrow-line spectrum (e.g., the one in Fig. 14) can be achieved only by resonance excitation: every other excitation method would produce broader spectra reflecting the plasma inhomogeneity. In particular, parametric resonance excitation in a system with two eigenfrequencies provides a mechanism to launch oscillations simultaneously at *both* eigenfrequencies (f_{pe} and f_{pi} in our case). It is true that parametric resonance excitation requires nonlinearity in the system, but this is not a problem, because nonlinearity is inherently present in all plasmas [47–49] and needs only larger amplitude signals to manifest itself. The eigenfrequencies of the collective ion and electron oscillations f_{LF} and f_{HF} in actual plasmas will be close, but not necessarily equal to f_{pi} and f_{pe} , the difference being due to the finite size of plasma and/or the corrections accounting for the large oscillation amplitudes [2,46,50].

The amplitude of ion and electron plasma oscillations can grow exponentially to very high levels (possibly gathering a few percent of the pump power) whenever conditions for parametric resonance are satisfied. This requires, first, a high-intensity oscillating E -field (to achieve large electron oscillation amplitude $x > \lambda_{De}$ as required for the existence of ion oscillations, and to provide nonlinearity for the parametric resonance), and second, an adequate tuning of the eigenfrequencies f_{HF} and f_{LF} relating to the frequency of the externally imposed electric field f_0 (the pump frequency), in the form of a *frequency-selection rule*. The frequency-selection rule for parametric resonance excitation requires, in general, that the sum or difference of eigenfrequencies (or some of their harmonics) be equal to the pumping frequency f_0 (or some of its harmonics). From experiment (Fig. 14), we are dealing with a particular case of such a selection rule (with no harmonics of f_0 or f_{HF} involved),¹³

$$f_0 = f_{HF} \pm n_{LF} f_{LF} \approx f_{pe} \pm n_{LF} f_{pi}, \quad n_{LF} = 0, 1, 2, \dots \quad (32)$$

The higher-order harmonics ($n_{LF} \geq 2$) of f_{LF} in Fig. 14 are weaker and eventually undetectable for $n_{LF} > 2$. This is

¹³The work in [2,46,50] examines only one permitted frequency-matching condition $f_0 = f_{HF} + f_{LF}$, following Nishikawa [49]. Nishikawa limits himself from the very beginning to relatively small E -field amplitudes, so that higher-order harmonics are excluded *a priori*. He further contemplates infinite homogeneous plasma (then considering f_{HF} and f_{LF} equal to f_{pe} and f_{pi} , respectively), and furthermore excludes $f_0 = f_{HF} - f_{LF}$ with the argument that waves of frequency below f_{pe} cannot propagate in such plasma, all limitations irrelevant to the strong fields in the finite (small-size) plasma from which the spectrum in Fig. [14] was taken.

because they arise only for large enough electron/ion oscillation amplitudes, i.e., very strong E -field, and, as a result, are often not considered in calculations [46,49]. Experimentally, parametric resonance excitation of electron and ion plasma oscillations can be achieved if one tunes the electron density n_e (and the ion density $n_i = n_e$) by varying the MW power level to meet the frequency selection rule (32) at some location(s) in the plasma [50].

The f_0 and f_{HF} EM emissions were detected in the microwave frequency range with an E -type antenna [Fig. 11(a)] and recorded on a spectrum analyzer, as shown in Fig. 14. The occurrence of such a strong signal at f_{HF} (only 10 dB below the pump power signal), meeting frequency selection rule (32), can only result from the parametric resonance mechanism described above, and indicates the existence of a particularly strong E -field intensity in the discharge. The two outer sidebands corresponding to $n_{LF} = 2$ indicate an E -field much stronger than what was considered theoretically in [49]. Additionally noteworthy in Fig. 14 is a noise-free MW spectrum extending down to a baseline of almost 50 dB below the f_0 power signal [50]. This is because the higher the E -field intensity, the larger the amplitude of the electron velocity entrained by the EM field with respect to the velocity thermal spread in the discharge kinetics, which is the source of noise.¹⁴

5. Localized electron heating in microdischarges

Microdischarges are a further example of inhomogeneous discharges where a high-intensity E -field is achieved in or close to the “inner volume.” They are defined as discharges where at least one dimension is in the submillimeter range [51]. The smallest dimension of a microdischarge is, in fact, set by the Debye length λ_{De} . With measured electron densities larger than 10^{14} cm^{-3} and average electron energies of approximately 1 eV at atmospheric pressure, a typical λ_{De} is less than $0.35 \mu\text{m}$ [51]. Such discharges have an extremely small inner volume V_i in terms of the inhomogeneous discharge model (Sec. VI B 1). The total plasma volume V_t , resulting from diffusion, driven by all kinds of gradients, always expands well beyond the electrode region whenever the latter is that small. It causes the power deposited in the inner volume to reach kW/cm^3 levels with only a few watts (or less) sustaining the discharge.

The maintenance E -field intensity in the inner volume is thus considerably larger than in homogeneous discharges, explaining the much higher electron density and much higher atomic/molecular excitation and dissociation rates encountered (Sec. VIB 3). The present general interpretation of microplasmas was proposed only recently [2,40], although these discharges had been extensively examined and reported before [51].

To be consistent with the foundations of the power-per-electron concept, the microdischarge considered here is generated by a MW field. The corresponding experimental

¹⁴It suggests that plasma antennas [12–14] could benefit from a much higher (transmission-reception) signal-to-noise ratio whenever the E -field intensity is raised through E -field confinement.

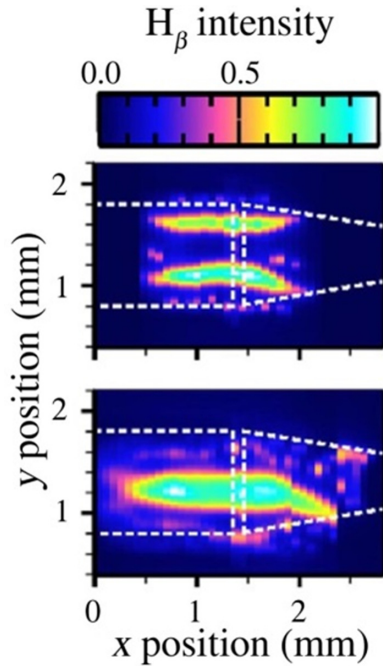


FIG. 15. Spatially resolved contour of the H_{β} line emission intensity showing that the argon microplasma extends outside the $100\ \mu\text{m}$ discharge gap and across the microstrip electrodes (outlined by dashed white lines). The single-resonator microdischarge is operated at $0.35\ \text{W}$ (top) and $0.62\ \text{W}$ (bottom) at $870\ \text{MHz}$ [41].

arrangements and results were worked out and documented by Hoskinson and Hopwood [41]. The discharge displayed in Fig. 15 is achieved in the $100\text{-}\mu\text{m}$ -wide gap between two microstrip electrodes, the open end of a single 1-mm -wide quarter-wavelength linear microstrip resonator on the left, and a grounded microstrip electrode on the right, operated in argon gas at atmospheric pressure and sustained at $870\ \text{MHz}$. The spatially resolved contour of the H_{β} line emission intensity recorded in the figure has been acquired with a CCD camera and realized with only a fraction of a watt of absorbed power. A plasma with an electron density of at least $2 \times 10^{14}\ \text{cm}^{-3}$ (determined from broadening of the H_{β} line) extends perpendicularly to the microstrip gap over approximately $1.2\ \text{mm}$ and thus encompasses a much larger volume compared to that of the $100\text{-}\mu\text{m}$ -wide interelectrode area, where the \mathbf{E} -field is localized. This system clearly corresponds to the definition given herein of inhomogeneous discharges where the absorption zone (the “inner volume” V_i) is (much) smaller than the whole plasma (the “total volume” V_t).

C. Discharge pulsed-operation as a means of achieving higher atomic and molecular excitation/dissociation and ionization rates

There are definite advantages in operating a discharge in pulsed mode relative to continuous-wave (CW) operation. Pertinent citations extracted from the literature report the following: (i) “pulsed plasma production can be used to produce plasma of high degree of ionization” [52]. Equivalently, “the time average electron density can be considerably higher than for a CW discharge for the same time-average

power” [53]; (ii) “in pulsed systems, new [operating] parameters appear over CW systems, specifically pulse duration t_{on} , pulse off-time t_{off} and duty cycle” $\delta = t_{\text{on}}/(t_{\text{on}} + t_{\text{off}})$ [52]; (iii) “it allows to control the ratio of charged to neutral species” [54,55]; (iv) “compared with operating in CW mode, higher instantaneous power allowing higher concentration of reactive species while reducing the plasma gas temperature effectively” [54]; (v) “lower heating of the plasma on pulsed operation is an indication that power losses are reduced” [56]; (vi) “ultrafast pulsation of microwaves allow(s) significant improvements of energy efficiencies during CO_2 splitting at atmospheric pressure as compared to CW operation of the microwave source” [57].

The various advantageous features of operating in pulsed mode [52,58] are best understood in terms of the power-per-electron and maintenance-field concepts, as proposed recently [2]. They are based on realizing that the intensity of the \mathbf{E} -field and electron energy decrease as pulse time elapses, ultimately down to their stationary values. Recall that under steady-state conditions, the power absorbed (and thus the maintenance \mathbf{E} -field intensity) adjusts exactly to compensate for the power losses as expressed by the power balance per electron, $\theta_A = \theta_L$ (26). Such a power balance is, however, not readily attained under pulsed-operation mode.

Consider the initial instant, immediately after the power pulse has been activated: only a few electrons have been generated, the power absorbed per electron, θ_A , is the largest of the pulse period, and the MW \mathbf{E} -field intensity is the highest. As electron density increases with elapsed pulse time, θ_A decreases and so does the \mathbf{E} -field intensity. As for the power lost per electron, θ_L , it is the lowest at the very start of the pulse [electron energy not high enough yet in (25)] but rises quickly with the elapsed pulse time. Then, depending on the duration of the pulse, either θ_A reaches in the end simply a minimum value, or, for a long enough pulse time, θ_A comes to stationarity. Therefore, at the beginning of the pulse, $\theta_A \gg \theta_L$ but, at long enough pulse duration time, both values become stationary, conforming to the power balance relation (26), $\theta_A = \theta_L$. This indicates that it is at (or very close to) the beginning of the pulse that the highest atomic and molecular excitation/dissociation and ionization rates are to be expected.

The next point to be addressed concerns the second pulse (or a succession of pulses) after an initial first pulse. When considering an isolated (solitary) pulse, it was taken for granted that there were no electrons in the discharge gas before the start of the pulse. Recovering the same high \mathbf{E} -field intensity at the immediate initiation of the second pulse would also require that no electrons be present. However, there are two practical limitations to such an issue: first, the pulse off-time (at zero MW power) needed for all charged particles to recombine might be too long for an economical plasma-driven process, and second, the MW power demanded for the discharge to reignite with zero initial electrons in the gas could exceed the power available from the MW generator (initial ignition can be achieved by some other means, not economical to repeat for each pulse). A possible intermediate solution with zero MW power in-between pulses is to set a high enough repetition rate (such that a zero-electron state is not reached before the next pulse) [59] or to maintain some minimum electron density in-between pulses at an idle

MW power level. Nonetheless, the lower the remnant electron density in-between pulses, the higher the E -field intensity at the beginning of the next pulse.

To isolate in the pulse mode the portion with the highest possible electric field strength (and be able to observe it), it is necessary to have a MW pulse generator capable of producing pulses with duration a fraction of that required for plasma formation, i.e., a few μs , and even shorter pulse rise times. An adequate temporal resolution of pulse observation furthermore necessitates time-resolved OES with gate times of a few tens of ns (or less). This was not possible with magnetron MW generators (where the usual rise time is of the order of tenths of μs), and therefore no such power measurements for θ_A and for the corresponding electron density were conducted at the Université de Montréal. Nowadays magnetrons can be advantageously replaced by solid-state MW devices [57,58]: for example, in [57], the square pulse and interpulse lengths are in the ranges 2.0–5.0 and 3.0–7.5 μs , respectively, with OES gate times as short as 20 ns.

Experimental results from Soldatov *et al.* [57,60] support the behavior expected from the power-per-electron concept, including the fact that the E -field intensity should be the highest at the beginning of the pulse. Citing their paper, “for the first time in atmospheric microwave plasma (CO₂ splitting case), two distinct regimes were observed along the energy pulses for the selected conditions: a nonequilibrium regime existing at the beginning of the pulse and a thermal equilibrium regime when the pulse surpasses approximately 1.6 μs of duration.” [It is possible to] “improve the efficiency by selecting suitable off-times.” As expected, in the reported observations the pulse duration and the off-time in-between pulses are the essential controlling features: the pulse start, as the E -field intensity decreases from its peak value, corresponds to a nonequilibrium regime, followed by an equilibrium regime when the E -field intensity has reached its stationary (lowest) value. This is in agreement with the behavior expected based on the power-per-electron concept, and it demonstrates the concept’s applicability to the analysis of both equilibrium and nonequilibrium situations.

Surface-wave sustained discharges under pulse-operating mode. For SWDs with pulsed-plasma generation, the power balance is no longer local since an ionization front with strong axial gradients and fluxes develops. During the pulse-on interval, an antenna-type EM radiation builds up near the field-applicator, which penetrates the (MW transparent) dielectric discharge tube, ionizing the gas inside it. Such a pulse-operating mode could yield valuable species stemming from the high-intensity E -field at the onset of the pulse, these species being possibly carried, through gas flow, to the extremity of an open-ended discharge tube for applications.

One more word is warranted about the occurrence of a sudden increase in the power supplied to an SWD. Coming back to Sec. II B and the sentence “increase in applied MW power ... does not modify the previously existing axial electron density gradient,” one should keep in mind that this sentence conceals what happens during the transient time period (μs timescale [61]) during which MW power is increased from, say, 200 to 250 W. The effect of the resulting power surge can be described in a similar way to that of the rise time of a pulse.

At the very beginning, the value of θ_A is greatest (a sudden larger absorbed power with low or almost zero preexisting electron density), which causes the SW E -field intensity to increase at the beginning of the SW plasma column. As a result, the wave propagates with a higher electric field strength along the column toward its end, where it is eventually reflected, forming a standing-wave pattern along the plasma column on its return path. As the electron density continues to increase as a function of time, the electric field intensity decreases accordingly, causing the standing-wave maxima and minima to become lower and lower, so that at the end, having reached the stationary state, the linear axial distribution of electron density is recovered.

VII. THE POWER-PER-ELECTRON CONCEPT APPLIED TO DISCHARGE SIMILARITY LAWS

The previous sections led to a better/more complete understanding of discharge mechanisms (e.g., microdischarges, pulsed-operated discharges). This section focuses on applying the power-per-electron concept to formulate similarity discharge laws.

Similarity laws make it possible to determine to what extent the operating conditions of a discharge can be modified without changing its characteristics. This leads to expressions or graphical representations where the product and/or quotient of two or three quantities appears to depend on a similar grouping of quantities. The similarity laws thus allow access to experimental or theoretical results without having to perform additional measurements or calculations.

Along those lines, Ferreira and Loureiro [30] showed that the long-time known E/p versus pR similarity law for dc discharges could be extended to SWDs in terms of θ/p versus pR . The theoretical argument for such a similarity law is briefly outlined in the Appendix.

The θ/p versus pR similarity law allows, among other things, determining the energy cost in terms of p and R for a given application. Although the power-per-electron concept is most useful with MW discharges, the θ_A value can serve to examine, regardless of the field frequency (even dc discharges), how much power is needed to maintain an electron-ion pair in a given discharge according to operating conditions (f , p , and R). Calculating the value of θ is straightforward only with microwave discharges; however, measured θ_A values from any other type of discharge can be used for quantitative appraisal of discharge efficiency and for highlighting possible common features.

Characterizing discharges with the θ parameter rather than with the E -field intensity has definite advantages. In that regard, three points are worth underlining: (i) Determining experimentally the intensity of the maintenance E -field of discharges implies ascertaining it with an antenna that enters the plasma, whereas measuring the value of θ can be made externally to the discharge through power measurements (Sec. III A: Experimental value of θ_A). The latter method is noninvasive and, therefore, more accurate; one gets the similarity law in terms that are easier to access. (ii) Expressing the similarity law in terms of θ instead of the E -field intensity prevents us from forgetting that the E -field intensity is an internal parameter, not an operator applied quantity. (iii) When the

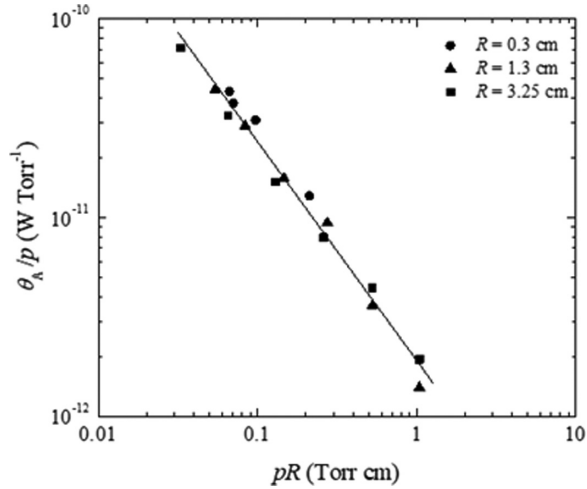


FIG. 16. Measured θ_A/p values as functions of the pR product for a SWD sustained in argon gas at reduced pressure ($pR < 1$ Torr cm) and 200 MHz that include three different values of the discharge tube radius R [42]. Logarithmic linearity of the similarity law firmly holds statistically since the coefficient of determination of its least-squares regression r^2 reaches 0.985.

EM field frequency sustaining the discharge is below typically 100 MHz, i.e., when ions are also picking up power directly from the HF E -field, expression (16) relating θ_A to the E -field intensity is no longer valid. Nonetheless, one can rely on the measured θ_A values, regardless of the kind of discharge, to analyze the influence of operating conditions on the discharge power cost, hence on the efficiency of a given plasma-driven process.

A. θ_A/p versus pR similarity law at low pressures

1. θ_A/p versus pR curves for microwave discharges

Figure 16 displays experimental points comprising three different R values [42] for a given SWD frequency. These data points all lie, with a high degree of statistical confidence, on the same straight line for the three different R -values, confirming the logarithmic linearity (power law) of the θ/p versus pR similarity law for SWDs at reduced gas pressures implying $pR \leq 1$ Torr cm.

Figure 17 illustrates a θ/p versus pR logarithmic plot where there are again three discharge tube radii, this time operated not at one but over several widely differing frequencies. The resulting graphic, in contrast to Fig. 16, displays three separate straight lines,¹⁵ each statistically well correlated to a distinct R value (r^2 is above 0.99 with all three curves) with their slope increasing, although only slightly, as the tube radius is decreased. From these observations, the following can be inferred:

(i) The θ/p versus pR logarithmic plot is not an absolute similarity diagram since it depends somehow on R .

¹⁵Figure 17 was previously reported [33,62] as a unique similarity law: however, a finer resolution of the experimental data using linear least-squares regressions revealed three distinct straight lines, as shown in the redrawn Fig. 17.

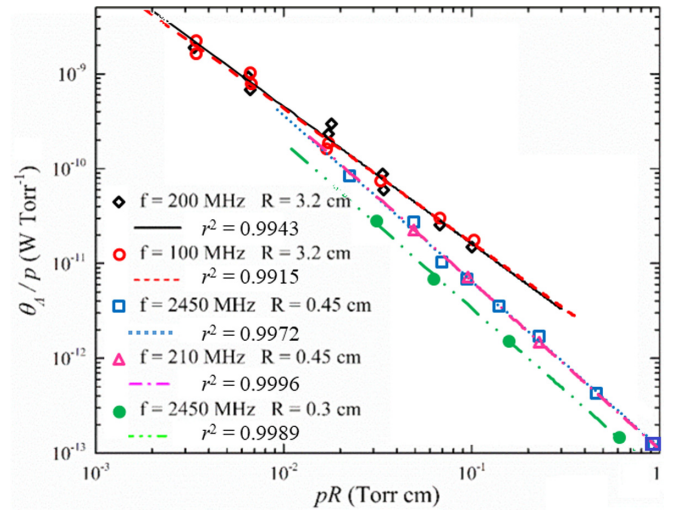


FIG. 17. Measured absorbed power per electron θ_A normalized to gas pressure p as a function of p times tube radius R with SWDs of different R and extended field frequencies f . The data for $R = 0.3$, 0.45, and 3.2 cm are from [25,63], and [62], respectively.

(ii) A smaller plasma radius contributes to an overall higher electron density as per Eq. (2) due to a higher axial gradient of electron density along the plasma column. This extends the electron density domain upwards and brings more stepwise ionization/excitation and more electron-electron collisions (and thus a more Maxwellian EEDF). Both effects enhance ionization and lower the average electron energy (ε) at the same value of pR (because the ionization needed to offset the diffusion loss of charged particles can now be achieved at a lower value of (ε)). The lower electron energy and the more energy-efficient stepwise ionization/excitation then give smaller values of θ_{LC} as per Eq. (25). This small decrease of θ/p with decreasing R (at fixed p) explains the *fine R structure* in Fig. 17.

(iii) The fact that this *fine R structure* is not observed in Fig. 16 is attributed to the limited electron density range (set by a single relatively low operating frequency), whereas in Fig. 17 the SW frequency range extends from 100 to 2450 MHz, and thus covers a much wider electron density range [recall that, per Eq. (3), in SWDs the minimal electron density increases with f^2]. This leads to θ/p varying by more than five orders of magnitude in Fig. 17, compared to only two orders of magnitude in Fig. 16. The limited θ/p range in Fig. 16 possibly prevented resolving the fine structure related to tube radius.

In conclusion, the θ/p versus pR logarithmic plot behaves as a similarity law provided the SWD operating conditions (and thus the electron density) are not too diverse: when θ/p is plotted over many orders of magnitude, a fine structure may be observed if measurements are accurate enough to resolve it.

2. The θ_A/p versus pR curves beyond microwave discharges

Gathering on one θ_A/p versus pR diagram the experimental data points from dc discharges and numerous SWDs (25–2450 MHz) allows us to appraise the respective relative power cost per generated electron-ion pair. While Fig. 17 presented

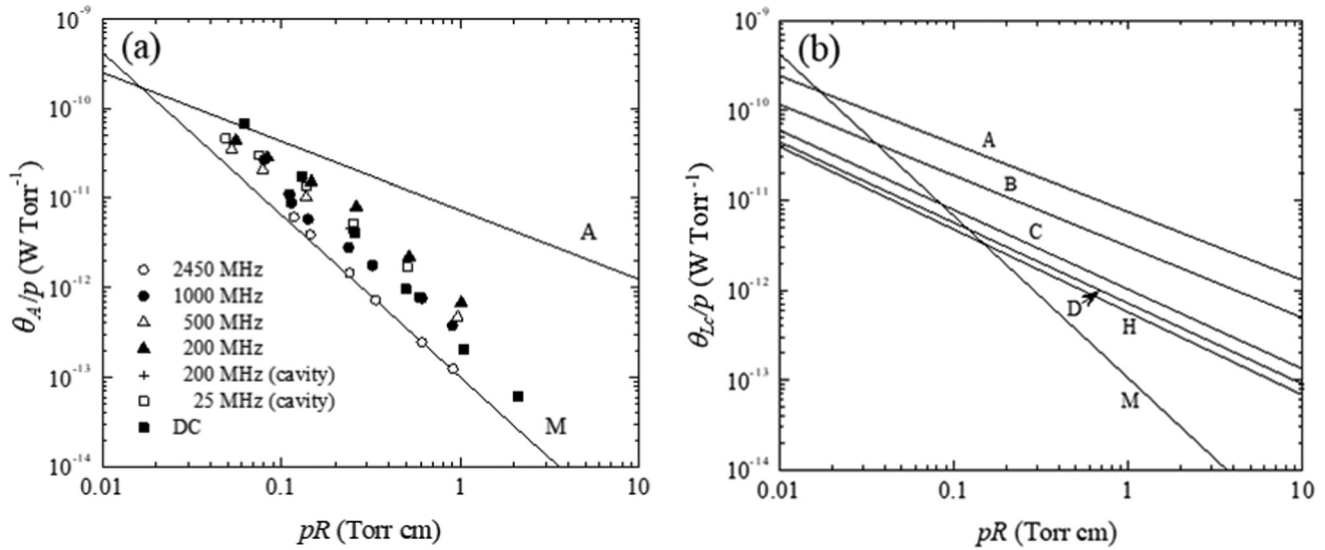


FIG. 18. (a) Experimental θ_A/p data as functions of pR from SWDs sustained at various frequencies (with corresponding R values varying by a factor of 3), and from the positive column of a dc discharge, all at reduced gas pressures ($pR \leq 1$ Torr cm) [42]. In the SWD case, the electron density required for determining θ_A is obtained by the phase variation of the surface wave E -field along the plasma column [64] or by means of a TM_{010} resonant cavity [44]; (b) set of θ_{Lc}/p values calculated as a function of pR considering different ν_{ce}/ω ratios where ω varies from ∞ to 0, A, $\nu_{ce}/\omega = \infty$ (dc case); B, $\nu_{ce}/\omega = 6.7$; C, $\nu_{ce}/\omega = 1.25$; D, $\nu_{ce}/\omega = 0.67$; and H, $\nu_{ce}/\omega = 0$ (MW case). Ambipolar diffusion regime and direct ionization from the ground state were assumed [42]. M, dominating electron-electron collisions, any ω value (Maxwellian EEDF).

θ_A/p versus pR plots for SWDs sustained at MW frequencies only, Fig. 18(a) further includes data points from dc discharges and from SWDs outside the microwave range down to 25 MHz, all at reduced gas pressures ($pR \leq 1$ Torr cm). Lower observed values of θ_A/p are attributed to the increase of the minimum and overall electron density of SWDs at higher frequencies [recall that at the column end its minimum is given by (3)]. Higher electron densities lead, as explained above in the discussion of Fig. 17, to lower values of θ/p , due to more stepwise ionization/excitation and more Maxwellian EEDF.

Recalling that relation (16) connecting θ_A to the E -field intensity no longer holds outside the microwave frequency domain, the main interest of this extended data set lies in the possibility to evaluate, as already mentioned, the power required to sustain an electron-ion pair in discharges in general. On a practical level, the observed dependence of the absorbed power θ_A on the field frequency explains, for instance, the well-known fact that it is far more power-efficient to operate an ion-plasma source at MW frequencies than at rf since θ_A then reaches its lowest value. Figure 18(a) also reveals that the data points, although related to a large variety of operating conditions (f , p , and R), do not deviate so much from an “averaged” straight line, suggesting a useful extended “loose” similarity law [42].

Figure 18(b) exhibits a series of calculated θ_{Lc}/p versus pR straight lines, each resulting from the EEDF procured under different electron-neutral collisions [42], thereby covering the SW frequency range between 25 and 2450 MHz and including a (low-electron density) dc discharge. This is

achieved by varying the collisional ratio ν_{ce}/ω ¹⁶ from infinity (dc case: curve A) down to (almost) zero (MW range case, labeled H). The M curve (Maxwellian EEDF) corresponds to dominant electron-electron collisions regardless of the value of ω . The ambipolar diffusion regime and direct ionization from the ground state are assumed in the calculations [42]. In the case of SWDs, the calculated power lost per electron through collisions θ_{Lc} is found to decrease with increasing wave frequency, in this case due to the changes of the EEDF tail at higher frequencies. The increase of electron density (3) and the related higher stepwise ionization, also important factors leading to better power efficiency at higher frequencies, are not taken into account in the calculated values from Fig. 18(b), but they are manifested in the measurements from Fig. 18(a), contributing to the difference between both figures, as explained below. As for the lowest possible θ_{Lc} value, it is reached with the Maxwellian EEDF at large enough pR products.

Range of electron density considered in the calculation of the A-curve in Fig. 18(b). In their modeling of the θ_{Lc}/p versus pR diagram, Ferreira and Loureiro [30] initially made the assumption that “the electron concentration is higher in a high-frequency discharge than in a low-frequency or a

¹⁶ ν_{ce} is essentially the value of the gas density N expressed in the same frequency unit as ω ; in the case of argon, $\nu_{ce}[\text{s}^{-1}] = 2 \times 10^{-7} N[\text{cm}^{-3}]$ [42]. For a given gas pressure p (same abscissa in Fig. 18 for fixed tube radius R), the A to H curves have the same value ν_{ce} but correspond to different frequencies ω in the ν_{ce}/ω ratio.

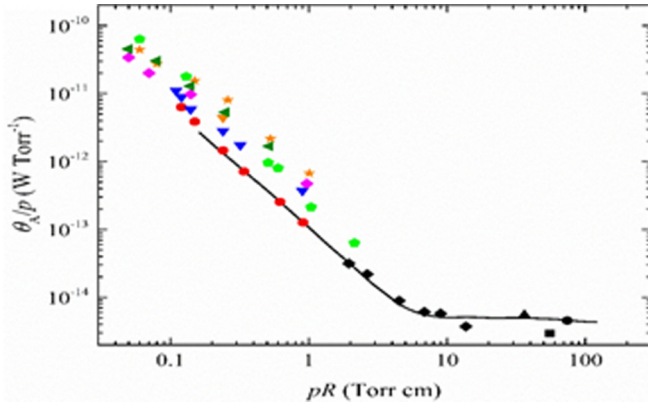


FIG. 19. Similarity-law curve θ_A/p vs pR covering the range from 0.03 to 75 Torr cm in argon. The solid line, calculated by Sá [65,66], considers a SWD with an electron density of 10^{14} cm^{-3} [65]. The atom density values N in her original (theoretical) θ/N vs NR similarity-law curve have been transformed to *converted* gas pressures p' assuming a gas temperature of 1500 K. The accompanying experimental points in black from SWDs, initially expressed as functions of N , were transformed into *converted* pressure values: (♦ [68]) $R = 1.75 \text{ mm}$, $f = 210 \text{ MHz}$, p from 50 to 200 Torr; (● [69]) (■ [70]) $R = 1 \text{ mm}$, $f = 2450 \text{ MHz}$ at atmospheric pressure; (▲ [24]) $R = 0.5 \text{ mm}$, $f = 2450 \text{ MHz}$ at atmospheric pressure. The colored symbols correspond to the experimental points in Fig. 18(a) at measured gas pressures: (●) $f = 2450 \text{ MHz}$, (▼) $f = 1000 \text{ MHz}$, (◀) $f = 500 \text{ MHz}$, (★) $f = 200 \text{ MHz}$, (▼) $f = 200 \text{ MHz}$ (cavity electron density measurements), (◆) $f = 25 \text{ MHz}$ (cavity), (◆) dc.

dc discharge for similar gas pressure and a given absorbed power per unit volume.” Given this, when calculating curve A (dc discharge), they assumed low electron density and therefore neglected stepwise ionization and electron-electron collisions, ignoring the Coulomb interaction. It turns out that in Fig. 18(a) the experimentally obtained dc points (■) are much closer to the calculated Maxwellian curve M than to curve A, suggesting that the electron density is higher than assumed by Ferreira and Loureiro in their calculations [30].

B. θ_A/p versus pR similarity law at and close to atmospheric pressure

By the late 1980s, a lot of attention had been paid in the SWD literature to the similarity law θ_A/p versus pR in the low-pressure range ($pR \leq 1 \text{ Torr cm}$), while no work had been done to document the corresponding behavior up to atmospheric pressure. It was Sá [65,66] who filled this gap by extending the initial and original low-pressure theoretical work of Ferreira and Loureiro [30]. Sá’s calculations published in [66] and reported in [24] considered that ionization occurred not only by direct impact of electrons on the (argon) atom in its ground state, but also by stepwise ionization, which was not surprising due to a higher electron density at such high gas pressures. Her original contribution was to incorporate in the calculations the presence of molecular ions (from argon atoms) with their losses by dissociative (volume) recombination, so that they participated in the depletion of charged

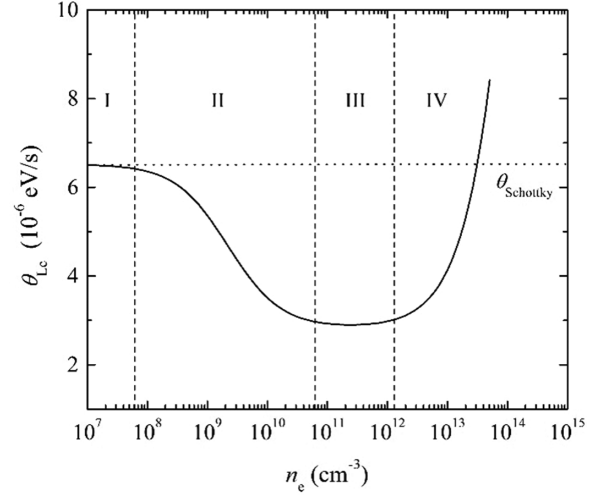


FIG. 20. Calculated power lost per electron θ_{Lc} in a surface-wave argon discharge as a function of n_e , identifying the specific electron density regions (I–IV) encountered when sweeping n_e through expression (33). Assumed conditions: $f = 144 \text{ MHz}$, $R = 14 \text{ mm}$, and $p = 0.5 \text{ Torr}$ ($\approx 67 \text{ Pa}$), after [72–74].

particles by ambipolar diffusion and atomic recombination [65]. Performed in small radius discharge tubes (to avoid contraction and filamentation effects at atmospheric pressure [67]), the calculated pR values ranged up to 70 Torr cm. Under such a larger range of pR values, $\log(\theta_A/p)$ is found to decrease initially linearly as a function of $\log(pR)$ up to $pR \approx 1 \text{ Torr cm}$ (Figs. 16–18) before turning, at higher pR values, into a horizontal θ_A/p plateau, as shown in Fig. 19.

Among all the colored data points in the figure, those at 2450 MHz fit the calculated curve best: endowed with the highest electron density [n_e increases with f^2 (3)], they are the closest to the assumed 10^{14} cm^{-3} electron density in Sá calculations.

Alves *et al.* [71] subsequently confirmed the essential role at atmospheric pressure of molecular ions on charged particle losses in the case of He SWDs. However, since they had to take into account lower electron densities than Sá ($5 \times 10^{12} \text{ cm}^{-3}$ in He rather than 10^{14} cm^{-3} in Ar), He_2^+ ions vanish mainly through diffusion, and not by dissociative recombination, which nevertheless leads to a similar abrupt change in the slope of θ_A/p versus pR past $pR \approx 1 \text{ Torr cm}$. Such behavior illustrates the relative importance of the mechanisms responsible for the production and loss of charged particles.

Another important (and somehow unexpected) experimental result is that, although the kinetic populating/depopping mechanisms are much more numerous at atmospheric pressure than at reduced pressures, the value of θ_A remains constant as a function of axial position [24]. This could possibly correspond to region III in Fig. 20 (below), where the electron density has become large enough for the stepwise ionization process to reach saturation, thus resulting in a constant value of θ_{Lc} as a function of n_e , and thus axial position along the SW plasma column.

C. Effect of electron density value: θ_{Lc} from ambipolar diffusion to volume recombination regime

It is possible to obtain better knowledge and additional practical features in the use of MW discharges by exploring computationally how the value of θ_{Lc} evolves in the transition from diffusion to recombination regime of charged particles. To do so, it is necessary to cover a sufficiently wide range of electron density to go from ambipolar diffusion to volume recombination while keeping track at the same time of the respective role of direct and multistep electron collisions leading to the ionization of atoms.

All the possible discharge conditions indicated above are taken into account in the following continuity equation, their specific importance emerging as the electron density increases [26]:

$$\nabla \cdot (D_a \nabla n_e) + v_{id} n_e + \frac{\rho_{ie} n_e^2}{1 + \eta n_e} - \alpha_{rm} n_e^2 = 0. \quad (33)$$

The first term corresponds to ambipolar diffusion losses (D_a is the ambipolar diffusion coefficient), the second term represents one-step ionization of atoms in the ground state (*direct ionization*), and the third term expresses in the nominator a two-step ionization process with rate coefficient ρ_{ie} , while in the denominator the coefficient η models ionization involving intermediate states with the possibility of accounting for their saturation ($\eta n_e \gg 1$, details in [26]). In the fourth term, the coefficient α_{rm} governs the volume recombination with molecular ions (dissociative recombination); this contribution is predominant compared to that of the volume recombination with atomic ions (not included) for gas pressures exceeding approximately 1 Torr (≈ 133 Pa).¹⁷

Figure 20 displays the value of θ_{Lc} calculated from (33) as a function of electron density, giving rise to four characteristic electron-density regions. At low electron density, the so-called Schottky condition (i.e., pure ambipolar diffusion and direct ionization only) yields region I in the figure. For higher n_e values (region II), the charged particles are still lost through ambipolar diffusion, but the stepwise ionization coming into play leads to a lowering of the average electron energy, and thus a decrease in the value of θ_{Lc} , as can be imagined from expression (25). For even higher values of n_e (region III), the loss of charged particles is still controlled by ambipolar diffusion, but the stepwise ionization process has come to saturation, giving a constant value of θ_{Lc} as a function of n_e . Finally, for still much higher electron densities (region IV), such that charged particles are lost both by ambipolar diffusion and volume recombination with the latter progressively taking over as n_e keeps on increasing, the value of θ_{Lc} strongly increases [72,73].

The fact that the minimum electron density of SWDs increases with f^2 leads to θ_{Lc} eventually tending to decrease with n_e , according to Fig. 20. This is in agreement with the

value of θ_{Lc} in Fig. 18(a) being lower at 2450 MHz than at 1000 MHz.

VIII. SUMMARY, DISCUSSION, AND CONCLUSION

Summary. The concept of power per electron that we have presented sheds light on the physics of discharges sustained by MW fields, highlighting some of their unique properties. The salient features of the power-per-electron concept can be summarized as follows: (i) The power balance is more than a simple question of equilibrium between the power lost in the plasma and the power absorbed in the discharge, as usually considered: We have indeed shown that the absorbed power adjusts to strictly compensate for the plasma losses, no matter how the power is being absorbed in the discharge. (ii) The MW \mathbf{E} -field intensity is an internal parameter, i.e., it is not fixed by the operator, but actually depends on θ_A (comprising E^2), once the value of θ_A has been set by the power balance $\theta_A = \theta_{Lc}$. (iii) It is possible to increase the intensity of the sustaining \mathbf{E} -field by confining it to a volume smaller than the plasma volume. A related aspect is that with the increase of \mathbf{E} -field intensity, the number of thermally driven electrons decreases with respect to those animated by the EM field: This results in a less and less “noisy” discharge best suited, for example, to provide plasma antennas with a higher signal-to-noise ratio. (iv) Analysis of the time evolution of θ_A during pulse mode operation of the discharge suggests that the \mathbf{E} -field intensity is highest at the very beginning of the pulse. (v) Ignoring the plasma sheath in the context of MW discharges is a well-justified approximation, because the sheath voltage is low, its dimension constant over time (because it cannot follow the variation of the EM \mathbf{E} -field), and its extent is small compared to the dimensions of the plasma (due to the relatively high electron densities in MW discharges).

Discussion. The concept of power per electron uses macroscopic variables, ensuring that the microscopic mechanisms are represented by average values stemming, for instance, from the electron energy distribution function (EEDF). In this respect, the concept is probably less detailed and not as complete as what kinetic models can provide, but it offers experimentalists and engineers a more synthetic approach to the physics of discharges, emphasizing the “physical images” of their mechanisms. The absence of a controllable sheath in MW discharges can be detrimental in optimizing or even achieving applications such as material processing (e.g., thin film deposition, etching, surface chemistry). Contrarily, the energy savings from not having to sustain a high-voltage sheath (as with rf capacitively coupled discharges) can yield higher electron densities and more efficient gas processes [75,76].

Conclusion. The power-per-electron concept developed has proven instrumental in displaying overlooked discharge properties/mechanisms and in enabling the interpretation of known observations yet not satisfactorily accounted for. It includes, for example, the extension of the E/p versus pR similarity law for dc discharges to its more generalized form θ_A/p versus pR , where determining θ_A instead of the \mathbf{E} -field inten-

¹⁷Even though the density of atomic ions is greater. This is because molecular ion recombination is a two-body process while that for atomic ions is a three-body process, therefore less probable [26]. Molecular ions are notably found in noble gas discharges.

sity is also less intrusive experimentally. While calculations of θ_A outside the MW range are no longer straightforward, the experimental values of θ_A , regardless of the kind of discharge, allow us to appraise, for given operating conditions, the power cost required for maintaining an electron-ion pair in the discharge and to possibly optimize a plasma-driven process.

ACKNOWLEDGMENTS

Our deepest thanks go to Nicolay Britun (Nagoya University, Japan), Maria Dolores Calzada (Universidad de Córdoba, Spain), Ana Lacoste (Université Grenoble–Alpes, France), and Émile Carbone (INRS–Énergie, Matériaux, Télécommunications, Varennes, Québec, Canada) for their critical analysis of the manuscript during its elaboration. Danielle Kéroack (Université de Montréal) and Mariam Rachidi are gratefully acknowledged for data processing. The editing and publication fee support by the Conseil de Recherche en Sciences Naturelles et en Génie (CRSNG) of Canada is recognized.

APPENDIX: THE SPECIFICS OF THE POWER BALANCE IN MW SURFACE-WAVE SUSTAINED PLASMA COLUMNS CONTRASTED TO CAPACITIVELY COUPLED RF DISCHARGES

The fact that n_e in SWDs is proportional to absorbed power is not trivial at all, actually being their main distinctive feature, which has made SWDs highly attractive for modeling and applications. Found experimentally [1], this behavior led naturally to the concept of power (lost θ_L or absorbed θ_A) per electron, depending on discharge conditions (pressure, tube radius, eventually frequency) but not on power. Such a concept is impossible if the electron density is not proportional to power, a situation encountered when both electrons and ions are picking power directly from the high-frequency \mathbf{E} -field.

Indeed, the power transferred from the \mathbf{E} -field to ions increases progressively as the applied frequency is lowered below approximately 100 MHz. This is the case of the capacitively coupled rf plasmas (CCPs), the focus of the famous book by Lieberman and Lichtenberg [77]. For CCPs, in the frequently encountered case of high applied rf voltage and prevailing stochastic electron heating, the electron density is proportional not to the power, but to its square root [77]. In such a situation, the concept of *power* per electron would be of limited use, since it would be not explicit, but implicit (the power per electron depending itself on the power). This may have been the reason why Lieberman and Lichtenberg [77], with their book focusing on CCPs, did not consider *power* per electron, but the more complex concept of average *energy* lost per *electron-ion pair* hitting the wall, which (after multiplication by the Bohm flux at the wall), leads in their concept to the total absorbed power at steady state. In [77], this energy has two components:

(i) The average energy lost by the actual electron-ion pairs hitting the wall ($\mathcal{E}_e + \mathcal{E}_i$ in the notation of [77]).

(ii) The average energy spent by electrons (not necessarily the same electrons that hit the wall) in the plasma bulk due to collisions (\mathcal{E}_c in their notation), a concept introduced earlier in, e.g., [63].

Both components were defined per one electron-ion pair hitting the wall, or per one ionization event (in the absence of bulk recombination both definitions are equivalent because the number of electron-ion pairs lost at the wall is equal to the number of electron-ion pairs created in the bulk). Below we denote the energy spent on the average in the formation of an ion-electron pair as W_i , following the notation in [63]. In SWDs, the collision energy loss per electron W_i is equal to θ_{Lc}/v_i ¹⁸ in the notation of Eq. (25) above. In Lieberman and Lichtenberg’s concept [77], to get the total power one must add to W_i the energy lost by electrons and ions when hitting the wall, $\mathcal{E}_e + \mathcal{E}_i$, of which the latter (\mathcal{E}_i) can be rather large in CCPs (often larger than the collisional loss W_i) due to the high sheath voltage. The beauty of the power balance in SWDs is that one can, but need not, account separately for the power absorbed by electrons and ions, for two reasons: First, ions do not pick energy directly from the MW field and therefore all MW power is absorbed (at first) only by electrons. Second, the sheath voltage is low and the power lost for sustaining it is usually negligible.

The specific of SWDs is that their ions do not gain energy *directly* from the MW electric field, due to its high frequency and prevailing orientation (parallel to the walls), so that all MW power is absorbed by electrons *only*. Ions still do gain energy from the MW field (and then lose it when hitting the wall), but only *indirectly*, with the electrons and the electrostatic plasma field acting as intermediaries. In summary, all MW power is first absorbed by electrons (θ_A), and then most of it (θ_{Lc}) is spent in collisions, a small part is lost by electrons hitting the wall, and the rest is transferred to the ions in two steps: the electrons sustain the electrostatic ambipolar field and the sheath voltage, and the ions get their energy from there. This is an important difference with CCPs, where not only electrons but also ions gain energy *directly* from the rf field, and one must distinguish between “electron power” and “total absorbed power” ([77], Sec. 11.2), the former being only a part of the latter. Therefore, unlike dc or capacitively coupled rf plasmas, in SWDs the *electron power* is the same as the *total absorbed power*, and both need not be distinguished.

This leads to the similarity law of SWDs. To get it, one has to recall that both θ_{Lc} and v_i are proportional to the gas density N , and therefore their ratio $W_i = \theta_{Lc}/v_i$ does not depend on N , but only on the electron temperature

$$W_i \equiv \theta_{Lc}/v_i = W_i(T_e) \quad (\text{A1})$$

(forgetting for the moment the subtleties of non-Maxwellian EEDFs, which do not change the general reasoning). Excluding at very high pressures and electron densities, the electron temperature T_e is determined by the product of gas density N and ambipolar diffusion length (proportional to the column radius R in long SWDs),

$$T_e = T_e(NR), \quad (\text{A2})$$

a relation coming from the balance of ionization in the plasma bulk and charged particle flux to the walls (Sec. 3.13 in

¹⁸Simply divide the power lost in unit volume ($\theta_{Lc}n_e$) by the frequency of ionization events in the same volume (v_in_e).

[26]). Therefore, (A1) can be written also as $W_i = W_i(NR)$. In SWDs, the energy electrons spend for sustaining the sheath and presheath, as well as the small energy lost by electrons hitting the wall [$(k_B T_e/2) \ln(M/m_e)$, $k_B T_e/2$ and $2k_B T_e$ per electron, respectively] are generally small compared to W_i and can usually be neglected ($\theta_L \approx \theta_{Lc}$). Even if this additional energy were not small, it could have been easily added to (A1) without changing anything much, since it too depends only on T_e . This is another difference with CCPs, where the sheath voltage $\Delta\Phi_{sh}$ depends strongly on power P (typical dependence $\Delta\Phi_{sh} \propto P^{1/2}$) and therefore a similarity law in the form (A1) exists only for the electron power, but not for the total discharge power. The *total* power per electron-ion pair in CCPs comprises the absorbed power density as an additional parameter entering via the sheath voltage $\Delta\Phi_{sh}$, destroying the explicit link between discharge conditions and θ . As a result, an explicit similarity law can be established in the form (A1) or (A3) only for the electron power, and therefore would be of little use in CCPs, because it would account for only some (often minor) portion of the total power in play.

In SWDs, with or without the approximation $\theta_L \approx \theta_{Lc}$, and with θ_A equal to θ_L in steady state (so that both are denoted θ), the *total* power per electron can be expressed from (A1) as $\theta = v_i W_i(T_e)$. Writing the ionization frequency v_i as the product $v_i = N K_i(T_e)$ of gas density N and ionization rate K_i brings then the power-per-electron similarity law in the form $\theta/N = K_i(T_e) W_i(T_e)$. Taking once more advantage of (A2), this becomes

$$\theta/N = f(NR). \quad (\text{A3})$$

To get to the more familiar $\theta/p = f(pR)$, one has to finally replace the gas density N by $p = N k_B T_g$ (implying fixed gas

temperature T_g , as discussed in Sec. II A 3). The fine details omitted in the derivation of (A3) (the effect of electron density value on EEDF via electron-electron and stepwise collisions, nonconstant gas temperature, radially nonuniform electron temperature, etc.) may then result in a fine structure, as seen in Fig. 17.

Such a convenient similarity law does not exist for CCPs because θ_{Lc} (or W_i) would account for only some (often minor) portion of the total power in play (the ions being responsible for the rest).¹⁹

The similarity law for the maintenance field E is easily obtained from (A3) using the link between absorbed power and electric field intensity $\overline{E^2}$ (16). After taking into account that v_m is proportional to N , from (16) and (A3) one gets $\overline{E^2}/(v_m^2 + \omega^2) = F(NR)$, or, in terms of pressure (at fixed gas temperature), $\overline{E^2}/(v_m^2 + \omega^2) = F(pR)$. This is the famous result that in SWDs the maintenance field E is an internal parameter, independent of power or axial position [2,21,33,35], but related to operating conditions, as discussed in Sec. VI. All this is based on (10), so it does not work for CCPs, because stochastic heating near the sheaths is not included. Therefore, a parallel result for the maintenance field is not found in Lieberman and Lichtenberg [77].

Another difference is that the global model from [77] implies spatially constant EEDF and thus does not apply to pressures higher than a Torr where the electron-energy relaxation length is significantly shorter than the discharge diameter, whereas the power-per-electron concept and the related similarity laws are valid at discharge gas pressures running from a few mTorr to atmospheric pressure.

¹⁹A similarity law E/p vs pR for dc can be related to θ/p vs pR provided the E -field and the absorbed power are those of the positive column only, this excluding energy acquired by ions in the various (e.g., cathode) sheaths.

-
- [1] V. M. M. Glaude, M. Moisan, R. Pantel, P. Leprince, and J. Marec, Axial electron-density and wave power distributions along a plasma-column sustained by the propagation of a surface microwave, *J. Appl. Phys.* **51**, 5693 (1980).
- [2] M. Moisan and H. Nowakowska, Contribution of surface-wave (SW) sustained plasma columns to the modeling of RF and microwave discharges, *Plasma Sources Sci. Technol.* **27**, 073001 (2018).
- [3] M. Moisan and Z. Zakrzewski, Plasma sources based on the propagation of electromagnetic surface waves, *J. Phys. D* **25**, 1025 (1991).
- [4] M. Moisan, Z. Zakrzewski, and R. Pantel, The theory and characteristics of an efficient surface wave launcher (surfatron) producing long plasma columns, *J. Phys. D* **12**, 219 (1979).
- [5] M. Moisan, P. Levif, and H. Nowakowska, Space-wave (antenna) radiation from the wave launcher (surfatron) before the development of the plasma column sustained by the EM surface wave: a source of microwave power loss, *AMPERE Newsletter* **98**, 9 (2019).
- [6] T. Fleisch, Y. Kabouzi, M. Moisan, J. Pollak, E. Castañós-Martínez, H. Nowakowska, and Z. Zakrzewski, Designing an efficient microwave-plasma source, independent of operating conditions, at atmospheric pressure, *Plasma Sources Sci. Technol.* **16**, 173 (2007).
- [7] A. Durocher-Jean, E. Desjardins, and L. Stafford, Characterization of a microwave argon plasma column at atmospheric pressure by optical emission and absorption spectroscopy coupled with collisional-radiative modelling, *Phys. Plasmas* **26**, 063516 (2019).
- [8] M. Moisan, Plasma columns generated by the propagation of an electromagnetic surface wave have no effect on the properties of the wave, which depend only on operating conditions: a shift in paradigm, [arXiv:2106.11404](https://arxiv.org/abs/2106.11404).
- [9] M. Moisan, R. Pantel, and J. Hubert, Propagation of surface wave sustaining a plasma column at atmospheric pressure, *Contrib. Plasma Phys.* **30**, 293 (1990).
- [10] G. Wendt, R. W. P. King, F. E. Borgnis, C. H. Papas, H. Bremmer, L. Hartshorn, and J. A. Saxton, *Elektrische Felder und Wellen/Electric Fields and Waves* (Springer, Berlin, 1958).

- [11] H. Nowakowska, M. Lackowski, and M. Moisan, Radiation losses from a microwave surface-wave (SW) sustained plasma source (surfatron), *IEEE Trans. Plasma Sci.* **48**, 2106 (2020).
- [12] G. G. Borg, J. H. Harris, N. M. Martin, D. Thorncraft, R. Milliken, D. G. Miljak, B. Kwan, T. Ng, and J. Kircher, Plasmas as antennas: Theory, experiment and applications, *Phys. Plasmas* **7**, 2198 (2000).
- [13] T. Naito, S. Yamaura, Y. Fukuma, and O. Sakai, Radiation characteristics of input power from surface wave sustained plasma antenna, *Phys. Plasmas* **23**, 093504 (2016).
- [14] F. Sadeghikia, M. T. Noghani, and M. R. Simard, Experimental study on the surface wave driven plasma antenna, *AEU-Int. J. Electron. Commun.* **70**, 652 (2016).
- [15] D. T. Tuma, A quiet uniform microwave gas discharge for lasers, *Rev. Sci. Instrum.* **41**, 1519 (1970).
- [16] Y. M. Aliev, A. G. Boev, and A. Shivarova, On the non-linear theory of a long gas discharge produced by an ionizing slow electromagnetic wave, *Phys. Lett.* **92**, 235 (1982).
- [17] M. S. Kovačević, L. Kuzmanović, M. M. Milošević, and A. Djordjevich, An estimation of the axial structure of surface-wave produced plasma column, *Phys. Plasmas* **28**, 023502 (2021).
- [18] B. Gordiets, M. Pinheiro, E. Tatarova, F. M. Dias, C. M. Ferreira, and A. Ricard, A travelling wave sustained hydrogen discharge: modelling and experiment, *Plasma Sources Sci. Technol.* **9**, 295 (2002).
- [19] I. Zhelyazkov and V. Atanassov, Axial structure of low-pressure high-frequency discharges sustained by travelling electromagnetic surface waves, *Phys. Rep.* **255**, 79 (1995).
- [20] M. Chaker, M. Moisan, and Z. Zakrzewski, Microwave and RF surface-wave sustained discharges as plasma sources for plasma chemistry and plasma processing, *Plasma Chem. Plasma Process.* **6**, 79 (1986).
- [21] Y. M. Aliev, H. Schlüter, and A. Shivarova, *Guided-Wave-Produced Plasmas* (Springer, Berlin, 2000).
- [22] S. Daviaud, C. Boisse-Laporte, P. Leprince, and J. Marec, Description of a surface-wave-produced microwave discharge in helium at low pressure in the presence of a gas flow, *J. Phys. D* **22**, 770 (1989).
- [23] M. Christova, E. Castañón-Martínez, M. D. Calzada, Y. Kabouzi, J. M. Luque, and M. Moisan, Electron density and gas temperature from line broadening in an argon surface-wave-sustained discharge at atmospheric pressure, *Appl. Spectrosc.* **58**, 1032 (2004).
- [24] M. D. Calzada, M. Moisan, A. Gamero, and A. Sola, Experimental investigation and characterization of the departure from local thermodynamic equilibrium along a surface-wave-sustained discharge at atmospheric pressure, *J. Appl. Phys.* **80**, 46 (1996).
- [25] M. Chaker, P. Nghiem, E. Bloyet, P. Leprince, and J. Marec, Characteristics and energy balance of a plasma column sustained by a surface wave, *J. Phys. Lett.* **43**, 71 (1982).
- [26] M. Moisan and J. Pelletier, *Physics of Collisional Plasmas: Introduction to High-Frequency Discharges* (Springer, Berlin, 2012).
- [27] O. Boudreault, S. Mattei, L. Stafford, J. Margot, M. Moisan, R. Khare, and V. M. Donnelly, Nonlocal effect of plasma resonances on the electron energy-distribution function in microwave plasma columns, *Phys. Rev. E* **86**, 015402(R) (2012).
- [28] I. D. Kaganovich, V. I. Dermidov, S. F. Adams, and Y. Raitses, Non-local collisionless and collisional electron transport in low-temperature plasma, *Plasma Phys. Controlled Fusion* **51**, 124003 (2009).
- [29] W. P. Allis and S. C. Brown, High-frequency electrical breakdown of gases, *Phys. Rev.* **87**, 419 (1952).
- [30] C. M. Ferreira and J. Loureiro, Characteristics of high-frequency and direct-current argon discharges at low pressures: a comparative analysis, *J. Phys. D* **17**, 1175 (1984).
- [31] M. Moisan, R. Pantel, A. Ricard, V. M. M. Glaude, P. Leprince, and W. P. Allis, Distribution radiale de la densité électronique et de la densité des atomes excités dans une colonne de plasma produite par une onde de surface, *Rev. Phys. Appl.* **15**, 1383 (1980).
- [32] M. Moisan, C. M. Ferreira, Y. Hajlaoui, D. Henry, J. Hubert, R. Pantel, A. Ricard, and Z. Zakrzewski, Properties and applications of surface wave produced plasmas, *Rev. Phys. Appl.* **17**, 707 (1982).
- [33] C. M. Ferreira and M. Moisan, The similarity laws for the maintenance field and the absorbed power per electron in low-pressure surface wave produced plasmas and their extension to HF plasmas in general, *Phys. Scr.* **38**, 382 (1988).
- [34] C. M. Ferreira, Modelling of a low-pressure plasma column sustained by a surface wave, *J. Phys. D* **16**, 1673 (1983).
- [35] Z. Zakrzewski, Conditions of existence and axial structure of long microwave discharges sustained by travelling waves, *J. Phys. D* **16**, 171 (1983).
- [36] J. Margot and M. Moisan, Surface wave sustained plasmas in static magnetic fields for study of ECR discharge mechanisms, in *Microwave Excited Plasmas*, edited by M. Moisan and J. Pelletier (Elsevier, Amsterdam, 1992).
- [37] J. Margot and M. Moisan, Electromagnetic surface-waves for a new approach to the investigation of plasmas produced at electron-cyclotron resonance (ECR), *J. Phys. D* **24**, 1765 (1991).
- [38] W. P. Allis, *Handbuch der Physik* (Springer, Berlin, 1956).
- [39] J. Margot, M. Moisan, and M. Fortin, Power required to maintain an electron in a discharge: its use as a reference parameter in magnetized high frequency plasmas, *J. Vac. Sci. Technol. A* **13**, 2890 (1995).
- [40] M. Moisan and H. Nowakowska, Achieving an intense enough maintenance electric field in a low-pressure discharge sustained by a microwave field under ambipolar diffusion regime such that periodic parametric instabilities are generated, *J. Phys. D* **48**, 455201 (2015).
- [41] A. R. Hoskinson and J. Hopwood, Spatially resolved spectroscopy and electrical characterization of microplasmas and switchable microplasma arrays, *Plasma Sources Sci. Technol.* **23**, 015024 (2014).
- [42] M. Moisan, C. Barbeau, R. Claude, J. M. Ferreira, J. Paraszczak, A. B. Sá, G. Sauv e, and M. R. Wertheimer, Radio-frequency or microwave plasma reactors - factors determining the optimum frequency of operation, *J. Vac. Sci. Technol. B* **9**, 8 (1991).
- [43] M. Moisan, Description and properties of an RF plasma used for study of parametric interaction of a strong E-M field with plasma, *Plasma Phys.* **16**, 1 (1974).
- [44] M. A. Heald and C. B. Wharton, *Plasma Diagnostics with Microwaves* (Wiley, New York, 1965).

- [45] T. Shirakava and H. Sugai, Plasma oscillation method for measurements of absolute electron density in plasma, *J. Appl. Phys.* **32**, 5129 (1993).
- [46] Y. M. Aliev and V. P. Silin, Plasma oscillations in a high-frequency electric field, *Sov. Phys. JETP* **21**, 601 (1965).
- [47] V. A. Bayley and D. F. Martyn, The influence of electric waves on the ionosphere, *London, Edinburgh, Dublin Philos. Mag. J. Sci.* **19**, 369 (1934).
- [48] A. V. Gurevich, Nonlinear effects in the ionosphere, *Phys. Usp.* **50**, 1091 (2007).
- [49] K. Nishikawa, II. Parametric plasmon-phonon interaction, *J. Phys. Soc. Jpn.* **24**, 1152 (1968).
- [50] M. Moisan and P. Leprince, Experimental evidence of parametric instabilities in an unmagnetized plasma subjected to a strong H.F. electric field, *Beiträge Plasmaphys.* **15**, 83 (1975).
- [51] F. R. Schoenbach and K. Becker, 20 years of microplasma research: a status report, *Eur. Phys. J. D* **70**, 29 (2016).
- [52] A. Anders, Fundamentals of pulsed plasmas for materials processing, *Surf. Coat. Technol.* **183** (2004).
- [53] M. A. Lieberman and S. Ashida, Global models of pulse-power-modulated high-density low-pressure discharges, *Plasma Sources Sci. Technol.* **5**, 145 (1996).
- [54] C. Chuan-Jie, L. Shou-Zhe, Z. Jialiang, and L. Dongping, Temporally resolved diagnosis of an atmospheric-pressure pulse-modulated argon surface wave plasma by optical emission spectroscopy, *J. Phys. D: Appl. Phys.* **51**, 025201 (2018).
- [55] H. Sugai, K. Nakamura, Y. Hikosaka, and M. Nakamura, Diagnostics and control of radicals in an inductively coupled etching reactor, *J. Vac. Sci. Technol. A* **13**, 887 (1995).
- [56] A. Rousseau, L. Tomasini, G. Gousset, C. Boisse-Laporte, and P. Leprince, Pulsed microwave discharge: a very efficient h atom source, *J. Phys. D* **27**, 2439 (1994).
- [57] S. Soldatov, G. Link, L. Silberer, C. M. Schmedt, E. Carbone, F. D'Isa, J. Jelonnek, R. Dittmeyer, and A. Navarrete, A time-resolved optical emission spectroscopy reveals nonequilibrium conditions for CO₂ splitting in atmospheric plasma sustained with ultrafast microwave pulsation, *ACS Energy Lett.* **6**, 124 (2021).
- [58] E. Carbone and S. Nidjam, Ultra-fast microwave plasma breakdown: evidence of various ignition modes, *Plasma Sources Sci. Technol.* **23**, 012001 (2014).
- [59] E. Carbone, N. Sadeghi, E. Vos, S. Hübner, E. van Veldhuizen, J. van Dijk, S. Nijdam, and G. Kroesen, Spatio-temporal dynamics of a pulsed microwave argon plasma: ignition and afterglow, *Plasma Sources Sci. Technol.* **24**, 015015 (2015).
- [60] S. Soldatov, E. Carbone, A. Kuhn, G. Link, J. Jelonnek, R. Dittmeyer, and A. Navarrete, Efficiency of a compact CO₂ coaxial plasma torch driven by ultrafast microwave power pulsing: stability and plasma gas flow dynamics, *J. CO₂ Utilization* **58**, 101916 (2022).
- [61] A. Hamdan, F. Valade, J. Margot, F. Vidal, and J. P. Matte, Space and time structure of helium pulsed surface-wave discharges at intermediate pressures (5–50 Torr), *Plasma Sources Sci. Technol.* **26**, 015001 (2017).
- [62] M. Chaker and M. Moisan, Large-diameter plasma columns produced by surface waves at radio and microwave frequencies, *J. Appl. Phys.* **57**, 91 (1985).
- [63] M. Chaker, P. Nghiem, E. Bloyet, P. Leprince, and J. Marec, *Étude d'une Décharge Créée par une Onde de Surface*, Internal Report No. LP 190 (Université Paris-XI, France, 1981).
- [64] J. Margot-Chaker, M. Moisan, Z. Zakrzewski, V. M. Glaude, and G. Sauvé, Phase sensitive methods to determine the wavelength of electromagnetic waves in lossy nonuniform media: the case of surface waves along plasma columns, *Radio Sci.* **23**, 1120 (1988).
- [65] A. B. Sá, *Modelização de plasmas produzidos por ondas de superfície. Aplicação ao argon*, Tese de Doutorado (doctoral thesis) (Instituto Superior Técnico, Universidade Técnica de Lisboa, Portugal, 1989).
- [66] A. B. Sá, Modeling of Surface Wave produced Discharges in Argon at Low to Intermediate Pressure, in *Microwave Discharges, Fundamentals and Applications*, edited by C. M. Ferreira and M. Moisan (Plenum, New York, 1993).
- [67] E. Castañón-Martínez and M. Moisan, Expansion/homogenization of contracted/filamentary microwave discharges at atmospheric pressure, *IEEE Trans. Plasma Sci.* **39**, 2192 (2011).
- [68] A. Granier, *Étude des décharges créées par onde de surface à moyenne et haute pression. Application à l'analyse chimique. Thèse d'Ingénieur-Docteur*, Laboratoire de Physique des Gaz et des Plasmas (Université Paris-Sud, Orsay, France, 1986).
- [69] A. Besner, *Développement d'une source à plasma d'onde de surface pour l'analyse chimique par spectrométrie d'émission atomique*, Ph.D. thesis (Département de Chimie, Université de Montréal, Quebec, 1990).
- [70] S. Lévesque, *Etude de l'effet de fréquence sur les caractéristiques d'un plasma entretenu par une onde de surface à des pressions voisines de l'atmosphère*, M.Sc. thesis (Département de physique, Université de Montréal, Quebec, 1991).
- [71] L. L. Alves, G. Gousset, and C. M. Ferreira, A collisional radiative model for microwave discharges in helium at low and intermediate pressures, *J. Phys. D* **25**, 1713 (1992).
- [72] K. Makasheva and A. Shivarova, Surface-wave-produced plasmas in a diffusion-controlled regime, *Phys. Plasmas* **8**, 836 (2001).
- [73] H. Schlüter and A. Shivarova, Travelling-wave-sustained discharges, *Phys. Rep.* **443**, 121 (2007).
- [74] I. Koleva, K. Makasheva, T. Paunská, H. Schlüter, A. Shivarova, and K. Tarnev, Guided-wave-produced plasmas, *Contrib. Plasma Phys.* **44**, 552 (2004).
- [75] Y. Kabouzi, M. Moisan, J. C. Rostaing, C. Trassy, D. Guérin, D. Kéroack, and Z. Zakrzewski, Abatement of perfluorinated compounds using microwave plasmas at atmospheric pressure, *J. Appl. Phys.* **93**, 9483 (2003).
- [76] J. C. Rostaing, F. Bryselbout, M. Moisan, and J. C. Parent, Méthode d'épuration des gaz rares au moyen de décharges électriques de haute fréquence, *C. R. Acad. Sci. Paris Série IV tome 1*, 99 (2000).
- [77] M. A. Lieberman and A. J. Lichtenberg, *Principles of Plasma Discharges and Material Processing* (Wiley-Interscience, Hoboken, NJ, 2005).